A novel linear uncertainty propagation method for nonlinear dynamics with interval process

Licong Zhang
Northwestern Polytechnical University School of Astronautics
Chunna Li
Northwestern Polytechnical University School of Astronautics
Hua Su
Northwestern Polytechnical University School of Astronautics
Xiaoding Wang
China Academy of Launch Vehicle Technology
Chunlin Gong (leonwood@nwpu.edu.cn)
Northwestern Polytechnical University School of Astronautics

Research Article

Keywords: nonlinear dynamics, time-varying uncertainty propagation, convex model, interval process, linearization method

Posted Date: June 3rd, 2022

DOI: https://doi.org/10.21203/rs.3.rs-1677116/v1

A novel linear uncertainty propagation method for nonlinear dynamics with interval process

Licong Zhang[1], Chunna Li[1], Hua Su[1], Xiaoding Wang[2], Chunlin Gong[1]✉

Abstract Interval process is a preferable model for time-varying uncertainty propagation of dynamic systems when only the range of uncertainties can be obtained. However, for nonlinear systems, except Monte Carlo (MC) simulation, there are still few efficient uncertainty propagation methods under the interval process model. This paper develops a non-intrusive and semi-analytical uncertainty propagation method, named 'Convex Model Linearization Method (CMLM)', by constructing a linearization formulation of a nonlinear system in a non-probabilistic sense. First, the criterion to evaluate the difference between the original system and the linearization formulation is derived, represented by discrepancy of middle-point, radius, and correlations of response. By minimizing these three parameters, the coefficients of linear equations will be optimized to obtain the linearization formulation of the original system. Then, the analytical equations are built to calculate uncertainty response under the interval process, without time-consuming analysis of the original system. To further improve the efficiency of the linearization process, Chebyshev-polynomial is introduced to approximate the nonlinear dynamic analysis. Two numerical examples that duffing oscillator and vehicle ride are set to tested the proposed CMLM. Compared to MC method, with comparable uncertainty response precision, the CMLM just need 1%-10% times of dynamic analysis of the nonlinear system. Furthermore, a practical launch vehicle ascent trajectory problem with black-box dynamics is solved by, respectively, the CMLM and MC method. The results verify the capacity of the CMLM to deal with black-box problems and show that the CMLM performs better in terms of accuracy, efficiency and robustness.

Keywords: nonlinear dynamics, time-varying uncertainty propagation, convex model, interval process, linearization method

✉ Corresponding author: leonwood@nwpu.edu.cn

1 Shaanxi Aerospace Flight Vehicle Design Key Laboratory, School of Astronautics, Northwestern Polytechnical University, Xi'an 710072, China

2 Research and Development Department, China Academy of Launch Vehicle Technology, Beijing 100076, China

1. Introduction

Dynamic response evaluation of nonlinear systems plays a significant role in various practical engineering. Conventionally, the evaluation is based on a deterministic condition, however, practically, any dynamic systems are in the presence of uncertainty. Under these uncertainties, the performances of the systems will be affected. Even a slight bias might cause a great change in the dynamic response. Therefore, in recent years, much research has recognized the importance of uncertainty problems and developed several uncertainty propagation methods for dynamic response evaluation [1-3].

Generally, the probabilistic model is widely applied in uncertainty problems, in which the uncertainties are quantified by stochastic variables with certain probability distributions. For uncertainty propagation of dynamic responses, some categories of probabilistic methods, have been established, including Monte Carlo (MC) simulation [4], linear methods and nonlinear methods. MC simulation is capable to provide a result which approaches the true probability distribution, but requires a high computational cost. Linear methods including local linearization [5,6] and statistical linearization [7] have advantages in simplicity and efficiency. Nonlinear methods, such as polynomial chaos expansion (PCE) [8-10], are developed for highly nonlinear systems. To apply all the aforementioned probabilistic methods, there is an essential premise that the precise probability distributions of uncertainties are available. However, in many practical engineering problems, due to limited experiment condition or lack of knowledge, there are always restrictions to obtain sufficient information of uncertainties. To remedy this limitation of probabilistic methods, many non-probabilistic methods have been developed [11-14].

Convex model theory [13] assumes that the imprecise parameters are enveloped into a convex set, and quantify them by some certain bounds rather than precise probability distributions. Thus, it is regarded as a powerful supplement to traditional probabilistic method, and so far, has been widely investigated in a great number uncertainty analysis area. A growing number of researchers apply the convex model to evaluate uncertain response of nonlinear systems, such as a wind turbine geared transmission system [15], rigid–flexible multibody systems [16] and an overhead crane [17]. Accordingly, various methods are developed. Wu et al. [18,19] introduced the Chebyshev inclusion functions into interval problems which can achieve high accuracy and efficiency. Li et al. [20] proposed

a higher-efficiency sparse regression method to reduce the computational cost of Chebyshev method. Fu et al. [21,22] proposed a polynomial surrogate method for rotor system under interval uncertainties. Wang et al. [23,24] proposed a Legendre-polynomial-based method and applied it to complicated multibody dynamic systems. Polynomial-approximation approaches are shown to be effective to improve efficiency and guarantee precision for interval uncertainty propagation.

The underlying assumption of the aforementioned methods is that the uncertainties are fully independent and time-invariant. Practically, the uncertainties may be of strong or weak correlation or dynamic characteristics. To quantify the correlation of interval uncertainties, several improved convex models are proposed, including multidimensional parallelepiped models (MPMs) [25,26] and a multidimensional ellipsoidal model (MEM) [27]. These models describe the correlation of uncertainties through different size and shape of convex models. Thus, they provide a potential approach to correlation analysis of dynamic response under correlated interval uncertainties. Essentially, the response is a kind of time-varying uncertain variable, and its values at different times are correlated interval variables. In the probabilistic model, such similar time-varying uncertainty can be described as a stochastic process, however, there has been few similar effective mathematical tools for convex model. To end this, Jiang [28] proposed a new non-stochastic quantification model for time-varying uncertainty, namely the ‘interval process’ or ‘non-probabilistic convex model process’. This model quantifies the time-varying uncertainties using lower and upper bound functions, and describe the correlations of the values at different times using the MEM. Thus, it still presents the advantages that only the variation bounds rather than the precise probability distributions are required. Then the model is soon applied to dynamic response evaluation, the vibrations of single-degree-of-freedom systems, multiple-degree-of-freedom system and continuum structures are analyzed under the interval process [29]. Therefore, based on the interval process model, non-probabilistic methods for uncertainty propagation of dynamic systems under correlated uncertainties and time-varying uncertainties can be established. Up to now, most of the existing methods are only applicable for linear systems. For nonlinear systems, except MC simulation [30], only a Karhunen-Loève (K-L) expansion method [31] has been proposed, in which an interval process in time domain is described by superposition of infinite deterministic time-related functions with uncorrelated interval coefficients. For an interval process

with weak time-correlation and long-duration, the K-L method may be computationally prohibitive due to ‘dimension disaster’.

In conclusion, the interval process model is a preferable non-probabilistic tool for uncertainty propagation of dynamic response. However, for nonlinear systems, there is a lack of an efficient method under the interval process model. In the probabilistic model, linear methods are known for their high efficiency. Among them, the statistical linearization method transforms a nonlinear system into an approximate linear formulation in some statistic sense. It presents advantages that the derivatives of dynamic systems are not required and the modification of original systems can be avoided [32].

This work proposes a linear method, called ‘convex model linearization method (CMLM)’, for nonlinear dynamics under the interval process model. The following novelty is realized: First an index is derived to evaluate the difference between a nonlinear system and its approximate linear formulation in a non-probabilistic sense using the characteristics of a convex model (middle-point, radius and correlation). Then, based on this index, a solving process of time-varying uncertainty propagation for nonlinear dynamics by linearizing the nonlinear system is developed. Meanwhile, analytical equations for calculating the uncertainty propagation of the linearized system are established to complete this process, and the Chebyshev-polynomial approximation is applied to reduce the times of analysis of the nonlinear system in this process, thus further improve the efficiency.

The paper continues in Section 2 with a statement of the nonlinear dynamics with time-varying uncertainty under the interval process model. Section 3 introduces the proposed CMLM in detail. The methods are tested in two numerical examples and a launch-vehicle (LV) ascent-trajectory problem in Section 4. Finally, conclusions are given in Section 5.

2. Nonlinear dynamics with time-varying interval uncertainties

Consider nonlinear dynamics with the time-varying interval uncertainties $\boldsymbol{\omega}^{\mathrm{I}}(t)$ and correlated initial interval uncertainties $\boldsymbol{x}_0^{\mathrm{I}}$. The expression can be represented as:

$$\begin{cases} \dot{\boldsymbol{x}}^{\mathrm{I}}(t) = \boldsymbol{f}\left(\boldsymbol{x}^{\mathrm{I}}(t), t\right) + \boldsymbol{B}(t)\boldsymbol{\omega}^{\mathrm{I}}(t) \\ \boldsymbol{x}^{\mathrm{I}}(t_0) = \boldsymbol{x}_0^{\mathrm{I}} \end{cases} \tag{1}$$

where $\boldsymbol{f}(\cdot)$ are nonlinear functions; The superscripts I denotes interval, and $\boldsymbol{B}(t)$ is the corresponding

input matrix. Under the interval uncertainties, the responses of the nonlinear system $\boldsymbol{x}^{\mathrm{I}}(t)$ are also time-varying interval variables. To quantify these interval variables, the following models are introduced to describe the correlated interval uncertainties and the time-varying interval uncertainties.

2.1. Correlated interval uncertainties description

Generally, interval variables are described by an interval model (IM) as shown in (a) and (c) of Fig. 1. In the IM, a single variable is described by its upper and lower bounds, and multidimensional problem is then represented as a 'multidimensional box'. However, the IM is not effective to quantify the correlations between uncertainties. To remedy the deficiency, some other convex models are proposed, and among them MEM is a well-performed model [33], as shown in (b) and (d) of Fig. 1. In the MEM, the correlation of the variables can be described by the shape of the ellipsoid.

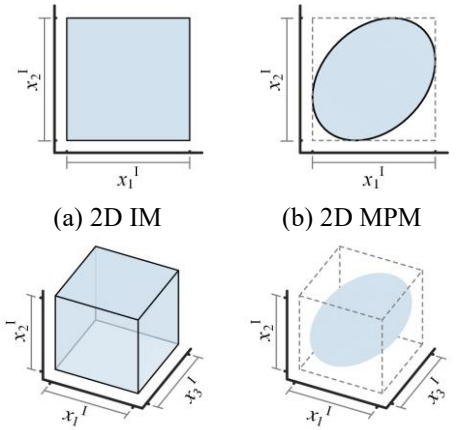

(a) 2D IM (b) 2D MPM

(c) 3D IM (d) 3D MPM

Fig. 1 The concepts of interval the model and the multidimensional ellipsoid model

For bivariant interval variables, $\boldsymbol{x}^{\mathrm{I}} = [x^{\mathrm{I}}_1, x^{\mathrm{I}}_2]$, the detailed definition of a 2D MEM and correlation between the two variables are illustrated in Fig. 2.

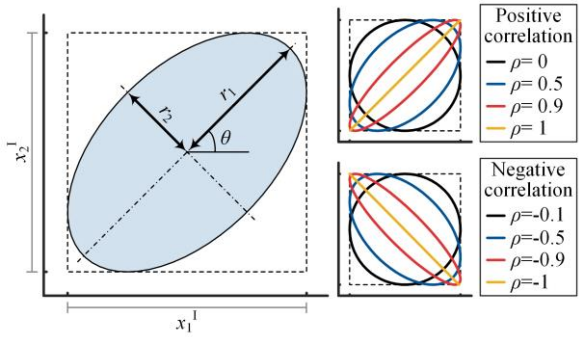

Fig. 2 The definition of correlation between interval variables in MEM

The 2D MEM degenerates into an ellipse defined as [27]:

$$\boldsymbol{x}^{\mathrm{I}}=\left\{\boldsymbol{x}\left|\left(\boldsymbol{x}-\boldsymbol{x}^{\mathrm{M}}\right)^{\mathrm{T}}\boldsymbol{G}\left(\boldsymbol{x}-\boldsymbol{x}^{\mathrm{M}}\right)\le 1\right.\right\} \tag{2}$$

where $\boldsymbol{G}$ is a 2 × 2 characteristic matrix. $\boldsymbol{x}^{\mathrm{M}}$ are middle points of $\boldsymbol{x}^{\mathrm{I}}$. Afterwards the covariance of x^{I}_1 and x^{I}_2 is defined by the geometry characteristics (θ, r_1, and r_2) of the ellipse as [29]:

$$\mathrm{Cov}\left(x_1^{\mathrm{I}},x_2^{\mathrm{I}}\right)=\sin(\theta)\cos(\theta)\left(r_1^2-r_1^2\right) \tag{3}$$

where θ denotes a rotation angle of the ellipse from its normal state as shown in Fig. 2, meanwhile r_1 and r_2 are the half lengths of the major axis and the minor axis of the ellipse. Naturally, the correlation coefficient is defined by (4)

$$\rho\left(x_1^{\mathrm{I}},x_2^{\mathrm{I}}\right)=\frac{\mathrm{Cov}\left(x_1^{\mathrm{I}},x_2^{\mathrm{I}}\right)}{x_1^{\mathrm{R}}x_2^{\mathrm{R}}} \tag{4}$$

The shapes of ellipse that correspond to several different correlation coefficients are shown in Fig. 2. When $|\rho|=1$, x^{I}_1 and x^{I}_2 are correlated and the ellipse degenerates into a line.

The bivariant covariance matrix $\boldsymbol{C}$ is defined as:

$$\boldsymbol{C}_{(2\times 2)}=\begin{bmatrix}\mathrm{Cov}\left(x^{\mathrm{I}}_1,x^{\mathrm{I}}_1\right) & \mathrm{Cov}\left(x^{\mathrm{I}}_1,x^{\mathrm{I}}_2\right)\\ \mathrm{Cov}\left(x^{\mathrm{I}}_2,x^{\mathrm{I}}_1\right) & \mathrm{Cov}\left(x^{\mathrm{I}}_2,x^{\mathrm{I}}_2\right)\end{bmatrix} \tag{5}$$

The diagonal elements of $\boldsymbol{C}$ are defined as variances of interval variables, which can be calculated as:

$$\begin{aligned}\mathrm{Cov}\left(x^{\mathrm{I}}_1,x^{\mathrm{I}}_1\right)&=D\left(x^{\mathrm{I}}_1\right)=\left(x_1^{\mathrm{R}}\right)^2\\ \mathrm{Cov}\left(x^{\mathrm{I}}_2,x^{\mathrm{I}}_2\right)&=D\left(x^{\mathrm{I}}_2\right)=\left(x_2^{\mathrm{R}}\right)^2\end{aligned} \tag{6}$$

And the characteristic matrix $\boldsymbol{G}$ of the ellipse in (2) are exclusively determined by covariance matrix $\boldsymbol{C}$ as follow:

$$\boldsymbol{G}=(\boldsymbol{C})^{-1} \tag{7}$$

For multi-dimensional problem, the covariance matrix is a $n \times n$ matrix as (8)

$$\boldsymbol{C}_{(n\times n)}=\begin{bmatrix}c_{11} & c_{12} & \cdots & c_{1n}\\ c_{21} & c_{22} & \cdots & c_{2n}\\ \vdots & \vdots & \ddots & \vdots\\ c_{n1} & c_{n2} & \cdots & c_{nn}\end{bmatrix} \tag{8}$$

where the elements of $\boldsymbol{C}$, c_{ij}, are the covariance of x^{I}_i and x^{I}_j as:

$$c_{ij}=\mathrm{Cov}\left(x^{\mathrm{I}}_i,x^{\mathrm{I}}_j\right)\quad i,j=1,2,\cdots,n \tag{9}$$

Eventually, the MEM can be determined by $\boldsymbol{C}$ as (10)

$$\boldsymbol{x}^{\mathrm{I}}=\left\{\boldsymbol{x}\left|\left(\boldsymbol{x}-\boldsymbol{x}^{\mathrm{M}}\right)^{\mathrm{T}}(\boldsymbol{C})^{-1}\left(\boldsymbol{x}-\boldsymbol{x}^{\mathrm{M}}\right)\le 1\right.\right\} \tag{10}$$

2.2. Interval Process Model

Based on the MEM, the interval process model [28,34] is proposed to describe a time-varying interval variable $x(t)$. At every time t, the value of $x(t)$ is an interval variable. Thus, the variation of $x(t)$ is enveloped within a pair of upper-bound and lower -bound functions, $x^{\mathrm{U}}(t)$ and $x^{\mathrm{L}}(t)$, as shown in Fig. 3. The interval process can be denoted as:

$$\left\{x^{\mathrm{I}}(t), t \in T\right\} \tag{11}$$

where T is called index set, which refers to time domain in time-varying uncertainty problem.

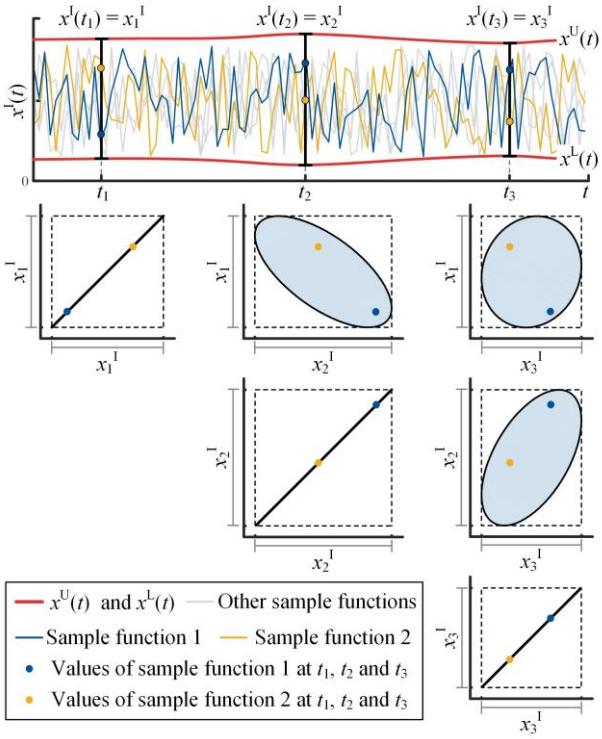

Fig. 3 The concepts of the interval process model

The middle-point function $x^{\mathrm{M}}(t)$ and radius function $x^{\mathrm{R}}(t)$ are defined as:

$$\begin{aligned} x^{\mathrm{M}}(t) &= M\left(x^{\mathrm{I}}(t)\right) = \frac{x^{\mathrm{L}}(t) + x^{\mathrm{U}}(t)}{2} \\ x^{\mathrm{R}}(t) &= R\left(x^{\mathrm{I}}(t)\right) = \frac{x^{\mathrm{U}}(t) - x^{\mathrm{L}}(t)}{2} \end{aligned} \tag{12}$$

For any times t_1 and t_2, the auto-covariance function of $x^{\mathrm{I}}(t)$ is defined as covariance of $x^{\mathrm{I}}(t_1)$ and $x^{\mathrm{I}}(t_2)$ based on MEM, as shown in Fig. 3.

$$C_{x^{\mathrm{I}}x^{\mathrm{I}}}(t_1, t_2) = \mathrm{Cov}\left(x^{\mathrm{I}}(t_1), x^{\mathrm{I}}(t_2)\right) \tag{13}$$

Similarly, the correlation-coefficient function is defined as:

$$\rho_{x^{\mathrm{I}}x^{\mathrm{I}}}(t_1,t_2)=\frac{C_{x^{\mathrm{I}}x^{\mathrm{I}}}(t_1,t_2)}{x^{\mathrm{R}}(t_1)x^{\mathrm{R}}(t_2)} \tag{14}$$

Moreover, for a set of interval processes, $\boldsymbol{x}^{\mathrm{I}}(t) = \{x^{\mathrm{I}}_1(t), x^{\mathrm{I}}_2(t),\ldots, x^{\mathrm{I}}_n(t)\}$, the cross-covariance function matrix is defined as:

$$\boldsymbol{C}_{\boldsymbol{x}^{\mathrm{I}}\boldsymbol{x}^{\mathrm{I}}}(t_1,t_2)=\begin{bmatrix} c_{11} & c_{12} & \cdots & c_{1n} \\ c_{21} & c_{22} & \cdots & c_{2n} \\ \vdots & \vdots & \ddots & \vdots \\ c_{n1} & c_{n2} & \cdots & c_{nn} \end{bmatrix} \tag{15}$$

where the elements c_{ij} is the covariance of $x^{\mathrm{I}}_i(t_1)$ and $x^{\mathrm{I}}_j(t_2)$ based on MEM as:

$$c_{ij}=\mathrm{Cov}\left(x^{\mathrm{I}}{}_i(t_1), x^{\mathrm{I}}{}_j(t_2)\right) \quad i,j=1,2,\cdots,n \tag{16}$$

When $t_1 = t_2 = t$, the diagonal elements of cross-covariance function matrix are defined as variance function:

$$\mathrm{diag}\left(\boldsymbol{C}_{\boldsymbol{x}^{\mathrm{I}}\boldsymbol{x}^{\mathrm{I}}}(t,t)\right)=D\left(\boldsymbol{x}^{\mathrm{I}}(t)\right)=\left(\boldsymbol{x}^{\mathrm{R}}(t)\right)^2 \tag{17}$$

If the middle point function $x^{\mathrm{M}}(t)$ and the radius function $x^{\mathrm{R}}(t)$ of an interval process $x^{\mathrm{I}}(t)$ are both constants and furthermore its auto-covariance function is only related to the time interval $\tau = |\, t_i - t_j \,|$ rather than the time points t_i and t_j, namely:

$$\begin{aligned} &x^{\mathrm{M}}(t)=m \\ &x^{\mathrm{R}}(t)=r \\ &C_{x^{\mathrm{I}}x^{\mathrm{I}}}(t_1,t_2)=C_{x^{\mathrm{I}}x^{\mathrm{I}}}(|t_1-t_2|)=C_{x^{\mathrm{I}}x^{\mathrm{I}}}(\tau) \end{aligned} \tag{18}$$

where m and r are both constants, then the interval process $x^{\mathrm{I}}(t)$ is defined as a stationary interval process. Similar to the stationary stochastic process, much physical phenomenon can be described by the stationary interval process in practical engineering.

Finally, under the interval process model, time-varying uncertainties $\boldsymbol{\omega}^{\mathrm{I}}(t)$ in the problem (1) can be describe by interval processes, and correlated interval initial uncertainties $\boldsymbol{x}_0{}^{\mathrm{I}}$ can be expressed as $\{\boldsymbol{x}_0 |\ (\boldsymbol{x}_0-\boldsymbol{x}_0{}^{\mathrm{M}})^{\mathrm{T}}(\boldsymbol{C}_{\boldsymbol{x}})^{-1}(\boldsymbol{x}_0-\boldsymbol{x}_0{}^{\mathrm{M}}) \le 1\}$ through the MEM. Under these uncertainties, the responses of the nonlinear system (1) are apparently interval processes represented by the upper-bound functions $\boldsymbol{x}^{\mathrm{U}}(t)$ and lower-bound functions $\boldsymbol{x}^{\mathrm{L}}(t)$, and the goal of uncertainty propagation is calculating $\boldsymbol{x}^{\mathrm{U}}(t)$ and $\boldsymbol{x}^{\mathrm{L}}(t)$.

3. The proposed CMLM

To achieve the uncertainty propagation through the CMLM. The criterion to evaluate the degree of approximation of a linear formulation to the original system is derived at first. Then the basic theory of time-varying uncertainty propagation for linear dynamics is established. Finally, the complete

uncertainty propagation process can be established.

3.1. Linearization of nonlinear dynamic system

Consider the nonlinear part of the system (1), $f(\boldsymbol{x}, u, t)$, under the interval process inputs, it becomes an interval process and its value at time t is an interval variable f^{I} as:

$$f\left(\boldsymbol{x}^{\mathrm{I}}, \boldsymbol{u}, t\right) = f^{\mathrm{I}} \tag{19}$$

Now try to replace the nonlinear part by an approximate linear equation, which is selected in a way to minimize the difference between it and the original equation. The linear equation, under interval uncertainties, is also an interval variable at time t as:

$$\hat{f}\left(\boldsymbol{x}^{\mathrm{I}}\right) = \boldsymbol{N}^{\mathrm{T}}\boldsymbol{r}^{\mathrm{I}} + \boldsymbol{M}^{\mathrm{T}}\boldsymbol{m} = \hat{f}^{\mathrm{I}} \tag{20}$$

where $\boldsymbol{x}^{\mathrm{I}} = \boldsymbol{r}^{\mathrm{I}} + \boldsymbol{m}$, thus, $\boldsymbol{r}^{\mathrm{I}}$ are interval parts with zero middle-point values, and $\boldsymbol{N}^{\mathrm{T}}$ is approximate linear state matrix of interval parts, meanwhile, $\boldsymbol{m}$ are middle-point parts with zero radius values, and $\boldsymbol{M}^{\mathrm{T}}$ is approximate linear state matrix of middle-point parts.

If the two interval responses of nonlinear and linear equation to the same interval inputs have minimum difference, the linear equation can be defined as the optimal approximation to the nonlinear equation in some non-probabilistic sense, or called convex-model sense. In the MEM, the differences between two interval variables can be evaluated by:

$$\begin{aligned} e_1 &= \left(f^{\mathrm{M}} - \hat{f}^{\mathrm{M}}\right)^2 \\ e_2 &= \left(f^{\mathrm{R}} - \hat{f}^{\mathrm{R}}\right)^2 \\ e_3 &= 1 - \rho\left(f^{\mathrm{I}}, \hat{f}^{\mathrm{I}}\right) \end{aligned} \tag{21}$$

where e_1 evaluates the difference in middle-point values, e_2 evaluates the difference in radius values, and e_3 evaluates the difference in correlation. Thus, the optimal approximate linear equation represented by $\boldsymbol{N}^*$ and $\boldsymbol{M}^*$ can be obtained by minimizing e_1, e_2, and e_3 simultaneously as:

$$\left\{\boldsymbol{N}^*, \boldsymbol{M}^*\right\} = \arg\min\left\{e_1, e_2, e_3\right\} \tag{22}$$

However, it is not convenient to calculate the correlation coefficient in the e_3 by the definition (4), due to that the geometry properties of the MEM cannot be obtained analytically. Literature [33] has proposed the sample correlation coefficient (SCC) which is capable to calculate the correlation coefficient between any two interval variables without constraint of the form of convex model as:

$$\rho_{\mathrm{s}}\left(x_i^{\mathrm{I}}, x_j^{\mathrm{I}}\right) = \frac{\sum_{s=1}^{N_{\mathrm{s}}}\left(x_i^{(\mathrm{s})} - x_i^{\mathrm{M}}\right)\left(x_j^{(\mathrm{s})} - x_j^{\mathrm{M}}\right)}{\sqrt{\sum_{s=1}^{N_{\mathrm{s}}}\left(x_i^{(\mathrm{s})} - x_i^{\mathrm{M}}\right)^2 \sum_{s=1}^{N_s}\left(x_j^{(\mathrm{s})} - x_j^{\mathrm{M}}\right)^2}} \tag{23}$$

where x^{I}_i and x^{I}_j are two interval variables; $x_i^{(\mathrm{s})}$, $x_j^{(\mathrm{s})}$ are sampling points of x^{I}_i and x^{I}_j. And $\rho_{\mathrm{s}} = \rho$, when the sampling points are uniformly distributed within a MEM.

Then, to obtain $\boldsymbol{N}^*$ and $\boldsymbol{M}^*$, the muti-objective optimization problem (22) can be transformed into a single-objective optimization problem as:

$$\begin{aligned} e &= e_1 + e_2 + e_3 \cdot 2 f^{\mathrm{R}} \hat{f}^{\mathrm{R}} \\ &= \left(f^{\mathrm{M}} - \hat{f}^{\mathrm{M}} \right)^2 + \left(f^{\mathrm{R}} - \hat{f}^{\mathrm{R}} \right)^2 + \left(1 - \rho_{\mathrm{s}} \left(f^{\mathrm{I}}, \hat{f}^{\mathrm{I}} \right) \right) \cdot 2 f^{\mathrm{R}} \hat{f}^{\mathrm{R}} \\ &= \left(f^{\mathrm{M}} - \hat{f}^{\mathrm{M}} \right)^2 + \left(f^{\mathrm{R}} \right)^2 + \left(\hat{f}^{\mathrm{R}} \right)^2 - 2\rho_{\mathrm{s}} \left(f^{\mathrm{I}}, \hat{f}^{\mathrm{I}} \right) \cdot f^{\mathrm{R}} \hat{f}^{\mathrm{R}} \end{aligned} \tag{24}$$

After simplification (see Appendix A for details), the expression can be obtained as:

$$e = \left(f^{\mathrm{M}} - \boldsymbol{M}\boldsymbol{m} \right)^2 + \left(f^{\mathrm{R}} \right)^2 + \boldsymbol{N}^{\mathrm{T}} \boldsymbol{C}_{\boldsymbol{x}^{\mathrm{I}}\boldsymbol{x}^{\mathrm{I}}} \boldsymbol{N} - 2\boldsymbol{\rho}_{\mathrm{s}} \left(f^{\mathrm{I}}, \boldsymbol{x}^{\mathrm{I}} \right) \cdot \mathrm{diag}\left(f^{\mathrm{R}} x_i^{\mathrm{R}} \right) \cdot \boldsymbol{N} \tag{25}$$

Minimization of e can be obtained when:

$$\begin{aligned} \frac{\partial e}{\partial \boldsymbol{M}} &= 2\left(M\left(f^{\mathrm{I}} \right) - \boldsymbol{M}^{\mathrm{T}} \boldsymbol{m} \right) \boldsymbol{m} = 0 \\ \frac{\partial e}{\partial \boldsymbol{N}} &= 2\boldsymbol{C}_{\boldsymbol{x}^{\mathrm{I}}\boldsymbol{x}^{\mathrm{I}}} \boldsymbol{N} - 2\boldsymbol{\rho}_{\mathrm{s}} \left(f^{\mathrm{I}}, \boldsymbol{x}^{\mathrm{I}} \right) \cdot \mathrm{diag}\left(f^{\mathrm{R}} x_i^{\mathrm{R}} \right) = 0 \end{aligned} \tag{26}$$

Thus, $\boldsymbol{N}^*$ and $\boldsymbol{M}^*$ can be calculated as:

$$\begin{aligned} \left(\boldsymbol{M}^* \right)^{\mathrm{T}} \boldsymbol{m} &= f^{\mathrm{M}} \\ \boldsymbol{N}^* &= \boldsymbol{C}_{\boldsymbol{x}^{\mathrm{I}}\boldsymbol{x}^{\mathrm{I}}}{}^{-1} \boldsymbol{\rho}_{\mathrm{s}} \left(f^{\mathrm{I}}, \boldsymbol{x}^{\mathrm{I}} \right) \cdot \mathrm{diag}\left(f^{\mathrm{R}} x_i^{\mathrm{R}} \right) \end{aligned} \tag{27}$$

And, the optimal approximate linear function can be expressed as:

$$\hat{f}\left(\boldsymbol{x}^{\mathrm{I}} \right) = \left(\boldsymbol{C}_{\boldsymbol{x}^{\mathrm{I}}\boldsymbol{x}^{\mathrm{I}}}{}^{-1} \boldsymbol{\rho}_{\mathrm{s}} \left(f^{\mathrm{I}}, \boldsymbol{x}^{\mathrm{I}} \right) \cdot \mathrm{diag}\left(f^{\mathrm{R}} x_i^{\mathrm{R}} \right) \right)^{\mathrm{T}} \boldsymbol{r}^{\mathrm{I}} + f^{\mathrm{M}} \tag{28}$$

Obviously, the approximate linear equation can be obtained by calculating the value of radius and middle-point of the nonlinear function under the interval inputs, and correlations between the interval response and interval inputs.

However, due to that the calculation of these values is based on the sampling points, a large amount computational cost of nonlinear functions is required. To reduce the cost, Chebyshev-polynomial approximation of the original function is applied.

A k-dimensional Chebyshev polynomial, for $x \in \{x_i | \, x_i^{\mathrm{L}} \le x_i \le x_i^{\mathrm{U}}, \, i = 1,2, \ldots, k \}$, is defined as [18]:

$$C_{n_1, n_2, \ldots, n_k}\left(x_1, x_2, \ldots, x_k \right) = \cos\left(n_1 \theta_1 \right) \cos\left(n_1 \theta_1 \right) \cdots \cos\left(n_k \theta_k \right) \tag{29}$$

where

$$\theta_i = \arccos\left(\frac{2x_i - \left(x_i^{\mathrm{L}} + x_i^{\mathrm{U}} \right)}{x_i^{\mathrm{U}} - x_i^{\mathrm{L}}} \right) \quad i = 1, 2, \ldots, k \tag{30}$$

Then, a k-dimensional function $f(\boldsymbol{x})$ can be approximated by Chebyshev polynomials with order no more than n as:

$$\begin{aligned} f(\boldsymbol{x}) &\approx p_n(\boldsymbol{x}) \\ &= \sum_{i_1,i_2,\ldots,i_k} c_{i_1,i_2,\ldots,i_k} C_{i_1,i_2,\ldots,i_k}(\boldsymbol{x}) \end{aligned} \tag{31}$$

where the coefficients $\boldsymbol{c}$ can usually be determined by two methods. The first one is Chebyshev tensor product method (CTPM)[35], and in the CTPM, the number of sampling points are no less than $(n+1)^k$. The CTPM can achieve the highest precision of the approximation, but for high-dimensional problems, computational efficiency will be extremely low. Another alternative construction form for Chebyshev-polynomial approximation is Chebyshev collocation method (CCM) [35] which requires only a portion of samples from the CTPM. The lowest number of samples m equals to:

$$m = \frac{(k+n)!}{k!n!} \tag{32}$$

In practice, the number of samples is usually selected as at least $2m$. Therefore, for low-dimensional problems (especially when $(n+1)^k < 2m$) CTPM is a better choice to construct Chebyshev-polynomial approximation, meanwhile, for high-dimensional conditions, CCM is a satisfied alternative method.

Afterwards, for a MEM domain, the Chebyshev-polynomial approximation should be constructed in a corresponding IM domain at first. Due to that the MEM domain is a subset of the IM domain for the same interval variables, the Chebyshev-polynomial approximation is also effective in the MEM domain. Next through a coordinate transformation method [28] (see Appendix B for details), take samples in the MEM domain, and scan to find the radius and middle-point of the response of the nonlinear function. Meanwhile, using the sampling points, the SCCs between the response and inputs can also be obtained by (23). Thus, the approximate linear function can be calculated through (28), and the whole process of linearization is concluded as follow:

Step 1 Define the order of Chebyshev polynomial n, and according the dimension of interval variables k, determine the number of interpolation points m for the construction of Chebyshev-polynomial approximation.

Step 2 Take m sets of interpolation points in IM domain of interval variables without consideration of correlation for the time being.

Step 3 Calculated the values of the nonlinear function at interpolation points. And construct

Chebyshev-polynomial approximation of the nonlinear function in the IM domain.

Step 5 Take samples in the ME domain through the coordinate transformation method (see Appendix B for details). And scan to calculated radius f^{R}, middle-point f^{M} using the Chebyshev-polynomial approximation, and calculate the SCCs $\boldsymbol{\rho}_{\mathrm{s}}(f^{\mathrm{I}}, \boldsymbol{x}^{\mathrm{I}})$ by (23).

Step 6 Calculate the approximate linear equation by (27).

3.2. Time-varying uncertainty propagation of linear dynamics

The general expression of a linear time-varying system can be expressed as:

$$\dot{\boldsymbol{x}}(t)=\boldsymbol{A}(t)\boldsymbol{x}(t)+\boldsymbol{B}(t)\boldsymbol{u}(t) \tag{33}$$

where $\boldsymbol{x}(t)$ are state variables, $\boldsymbol{A}(t)$ is state matrix, and $\boldsymbol{u}(t)$ are inputs, $\boldsymbol{B}(t)$ is corresponding input matrix. The solution of the problem with initial states $\boldsymbol{x}(t_0)$ can be expressed as:

$$\boldsymbol{x}(t)=\boldsymbol{\Phi}(t,t_0)\boldsymbol{x}(t_0)+\int_{t_0}^{t}\boldsymbol{\Phi}(t,\tau)\boldsymbol{B}(\tau)\boldsymbol{u}(\tau)d\tau \tag{34}$$

where, $\boldsymbol{\Phi}(t,t_0)$ is defined as state transition matrix, which satisfies the following property:

$$\boldsymbol{\Phi}(t_2,t_1)\boldsymbol{\Phi}(t_1,t_0)=\boldsymbol{\Phi}(t_2,t_0) \tag{35}$$

When the inputs to the system are uncertainty and described as interval processes $\boldsymbol{u}^{\mathrm{I}}(t)$, the responses are also transformed to interval processes as [36]:

$$\boldsymbol{x}^{\mathrm{I}}(t)=\boldsymbol{\Phi}(t,t_0)\boldsymbol{x}^{\mathrm{I}}(t_0)+\int_{t_0}^{t}\boldsymbol{\Phi}(t,\tau)\boldsymbol{B}(\tau)\boldsymbol{u}^{\mathrm{I}}(\tau)d\tau \tag{36}$$

Based on the theories of differential and integral of the interval process [29,36], the middle-point functions $\boldsymbol{x}^{\mathrm{M}}(t)$ can be calculated as:

$$\begin{aligned}\boldsymbol{x}^{\mathrm{M}}(t)&=M\left(\boldsymbol{x}^{\mathrm{I}}(t)\right)\\&=M\left(\boldsymbol{\Phi}(t,t_0)\boldsymbol{x}^{\mathrm{I}}(t_0)+\int_{t_0}^{t}\boldsymbol{\Phi}(t,\tau)\boldsymbol{B}(\tau)\boldsymbol{u}^{\mathrm{I}}(\tau)d\tau\right)\\&=\boldsymbol{\Phi}(t,t_0)M\left(\boldsymbol{x}_0^{\mathrm{I}}\right)+\int_{t_0}^{t}\boldsymbol{\Phi}(t,\tau)\boldsymbol{B}(\tau)M\left(\boldsymbol{u}^{\mathrm{I}}(\tau)\right)d\tau\\&=\boldsymbol{\Phi}(t,t_0)\boldsymbol{x}_0^{\mathrm{M}}+\int_{t_0}^{t}\boldsymbol{\Phi}(t,\tau)\boldsymbol{B}(\tau)\boldsymbol{u}^{\mathrm{M}}(\tau)d\tau\end{aligned} \tag{37}$$

And the cross-covariance function matrix can be calculated as:

$$\begin{aligned}\boldsymbol{C}_{\boldsymbol{x}^{\mathrm{I}}\boldsymbol{x}^{\mathrm{I}}}(t_1,t_2)=&\boldsymbol{\Phi}(t_1,t_0)\boldsymbol{C}_{\boldsymbol{x}^{\mathrm{I}}\boldsymbol{x}^{\mathrm{I}}}(t_0,t_0)\boldsymbol{\Phi}^{\mathrm{T}}(t_1,t_0)\\&+\int_{t_0}^{t_1}\int_{t_0}^{t_2}\boldsymbol{\Phi}(t_1,\tau_1)\boldsymbol{B}(\tau_1)\boldsymbol{C}_{\boldsymbol{u}^{\mathrm{I}}\boldsymbol{u}^{\mathrm{I}}}(\tau_1,\tau_2)\boldsymbol{B}^{\mathrm{T}}(\tau_2)\boldsymbol{\Phi}^{\mathrm{T}}(t_2,\tau_2)d\tau_1 d\tau_2\end{aligned} \tag{38}$$

where, $\boldsymbol{C}_{\boldsymbol{u}^{\mathrm{I}}\boldsymbol{u}^{\mathrm{I}}}(\cdot)$ is the cross-covariance function matrix of $\boldsymbol{u}^{\mathrm{I}}(t)$. Then the variance functions can be obtained when $t_1 = t_2 = t$ as:

$$
\begin{aligned}
D\left(\boldsymbol{x}^{\mathrm{I}}(t)\right) &= \operatorname{diag}\left(\boldsymbol{C}_{\boldsymbol{x}^{\mathrm{I}}\boldsymbol{x}^{\mathrm{I}}}(t,t)\right) \\
&= \operatorname{diag}\left(\boldsymbol{\Phi}(t,t_0)\boldsymbol{C}_{\boldsymbol{x}^{\mathrm{I}}\boldsymbol{x}^{\mathrm{I}}}(t_0,t_0)\boldsymbol{\Phi}^{\mathrm{T}}(t,t_0)\right) \\
&\quad + \operatorname{diag}\left(\int_{t_0}^{t}\int_{t_0}^{t}\boldsymbol{\Phi}(t,\tau_1)\boldsymbol{B}(\tau_1)\boldsymbol{C}_{\boldsymbol{u}^{\mathrm{I}}\boldsymbol{u}^{\mathrm{I}}}(\tau_1,\tau_2)\boldsymbol{B}^{\mathrm{T}}(\tau_2)\boldsymbol{\Phi}^{\mathrm{T}}(t,\tau_2)d\tau_1 d\tau_2\right)
\end{aligned}
\tag{39}
$$

Finally, the radius functions can be calculated as:

$$
\begin{aligned}
\boldsymbol{x}^{\mathrm{R}}(t) &= \sqrt{D\left(\boldsymbol{x}^{\mathrm{I}}(t)\right)} \\
&= \sqrt{\operatorname{diag}\left(\boldsymbol{\Phi}(t,t_0)\boldsymbol{C}_{\boldsymbol{x}^{\mathrm{I}}\boldsymbol{x}^{\mathrm{I}}}(t_0,t_0)\boldsymbol{\Phi}^{\mathrm{T}}(t,t_0)\right)} \\
&\quad + \sqrt{\operatorname{diag}\left(\int_{t_0}^{t}\int_{t_0}^{t}\boldsymbol{\Phi}(t,\tau_1)\boldsymbol{B}(\tau_1)\boldsymbol{C}_{\boldsymbol{u}^{\mathrm{I}}\boldsymbol{u}^{\mathrm{I}}}(\tau_1,\tau_2)\boldsymbol{B}^{\mathrm{T}}(\tau_2)\boldsymbol{\Phi}^{\mathrm{T}}(t,\tau_2)d\tau_1 d\tau_2\right)}
\end{aligned}
\tag{40}
$$

3.3. Uncertainty propagation process of nonlinear dynamics

Through the CMLM, the nonlinear dynamics with time-varying interval uncertainties can be transformed into an approximate linear problem as:

$$
\dot{\boldsymbol{x}}^{\mathrm{I}}(t) = \boldsymbol{N}^{\mathrm{T}}\boldsymbol{r}^{\mathrm{I}}(t) + \boldsymbol{M}^{\mathrm{T}}\boldsymbol{m}(t) + f^{\mathrm{M}}(t) + \boldsymbol{B}(t)\boldsymbol{\omega}^{\mathrm{I}}(t) \tag{41}
$$

The middle-point function and radius function of the linear problem can be obtained through (37) and (40). However, the known middle-point and covariance are required previously before the linearization through the CMLM. Therefore, the problem can only be solved discretely and iteratively.

To illustrate the iterative process, it is assumed that the linearization and calculation of previous i-1 discrete time points have been finished, and N_1^*, N_2^*, …, $N_{i\text{-}1}^*$ are obtained as:

$$
\left\{\boldsymbol{N}^* \middle| N_k^*, k = 1,2,\cdots,i-1\right\} \tag{42}
$$

Thus, the system can be regarded as a piecewise-linear problem, and the state transition matrix, from t_0 to $t_{i\text{-}1}$, can be expressed as:

$$
\boldsymbol{\Phi}^*(t_{i-1},t_0) = e^{\boldsymbol{N}_{i-1}^*(t_{i-1}-t_{i-2})}e^{\boldsymbol{N}_{i-2}^*(t_{i-2}-t_{i-3})}\cdots e^{\boldsymbol{N}_1^*(t_1-t_0)}\boldsymbol{I} \tag{43}
$$

Then, began to calculate the response of system at time t_i, and accomplish the linearization. First, scan to calculate the middle-point function at time t_i, $\boldsymbol{x}^{\mathrm{M}}(t_i)$. Take samples in MEM domain of $\boldsymbol{x}^{\mathrm{I}}(t_{i\text{-}1})$, and solve ordinary differential equation (ODE) problems from $t_{i\text{-}1}$ to t_i at these sampling points, by numerical ODE methods as:

$$
\boldsymbol{x}^{(\mathrm{s})}(t_i) = f_{\mathrm{ODE}}\left(\boldsymbol{x}^{(\mathrm{s})}(t_{i-1}), t_{i-1}\right) \tag{44}
$$

where $f_{\mathrm{ODE}}(\cdot)$ denotes an iterative step of an arbitrary numerical ODE method. And $\boldsymbol{x}^{\mathrm{M}}(t_i)$ can be obtained by scanning method as:

$$
\boldsymbol{x}^{\mathrm{M}}(t_i) = \frac{\max\left(\boldsymbol{x}^{(\mathrm{s})}(t_i)\right) + \min\left(\boldsymbol{x}^{(\mathrm{s})}(t_i)\right)}{2} \tag{45}
$$

It should be noted that Chebyshev-polynomial approximation can also be applied here to reduce the

computational cost of the scanning method. Consequently, calculate the covariance matrix function. Initialize N_i, let:

$$N_i^{\,0} = N_{i-1}^{\,*} \tag{46}$$

The state transition matrix, from t_0 to t_i, can be updated, by the property (35), as:

$$\boldsymbol{\Phi}^0(t_i,t_0) = e^{\boldsymbol{N}_i^{\,0}(t_i-t_{i-1})}\boldsymbol{\Phi}^*(t_{i-1},t_0) \tag{47}$$

Accordingly, the covariance matrix function can be calculated, by (38), as:

$$\begin{aligned}\boldsymbol{C}_{\boldsymbol{x}^{\mathrm{I}}\boldsymbol{x}^{\mathrm{I}}}{}^{(0)}(t_i,t_i) = &\boldsymbol{\Phi}^{(0)}(t_i,t_0)\boldsymbol{C}_{\boldsymbol{x}^{\mathrm{I}}\boldsymbol{x}^{\mathrm{I}}}(t_0,t_0)\left(\boldsymbol{\Phi}^{(0)}(t_i,t_0)\right)^{\mathrm{T}}\\ &+\int_{t_0}^{t_i}\int_{t_0}^{t_i}\boldsymbol{\Phi}^{(0)}(t_i,\tau_1)\boldsymbol{B}(\tau_1)\boldsymbol{C}_{\boldsymbol{u}^{\mathrm{I}}\boldsymbol{u}^{\mathrm{I}}}(\tau_1,\tau_2)\boldsymbol{B}^{\mathrm{T}}(\tau_2)\left(\boldsymbol{\Phi}^{(0)}(t_i,\tau_2)\right)^{\mathrm{T}}d\tau_1 d\tau_2\end{aligned} \tag{48}$$

It is not necessary to calculate the integration from initial time t_0, the results can be derived from the obtained covariance matrix at previous time point t_i-1 as:

$$\begin{aligned}\boldsymbol{C}_{\boldsymbol{x}^{\mathrm{I}}\boldsymbol{x}^{\mathrm{I}}}{}^{(0)}(t_i,t_i) = &e^{\boldsymbol{N}_i^{\,0}(t_i-t_{i-1})}\boldsymbol{C}_{\boldsymbol{x}^{\mathrm{I}}\boldsymbol{x}^{\mathrm{I}}}(t_{i-1},t_{i-1})\left(e^{\boldsymbol{N}_i^{\,0}(t_i-t_{i-1})}\right)^{\mathrm{T}}\\ &+\int_{t_0}^{t_{i-1}}\int_{t_{i-1}}^{t_i}\boldsymbol{\Phi}^{(0)}(t_i,\tau_1)\boldsymbol{B}(\tau_1)\boldsymbol{C}_{\boldsymbol{u}^{\mathrm{I}}\boldsymbol{u}^{\mathrm{I}}}(\tau_1,\tau_2)\boldsymbol{B}^{\mathrm{T}}(\tau_2)\left(\boldsymbol{\Phi}^{(0)}(t_i,\tau_2)\right)^{\mathrm{T}}d\tau_1 d\tau_2\\ &+\int_{t_{i-1}}^{t_i}\int_{t_0}^{t_{i-1}}\boldsymbol{\Phi}^{(0)}(t_i,\tau_1)\boldsymbol{B}(\tau_1)\boldsymbol{C}_{\boldsymbol{u}^{\mathrm{I}}\boldsymbol{u}^{\mathrm{I}}}(\tau_1,\tau_2)\boldsymbol{B}^{\mathrm{T}}(\tau_2)\left(\boldsymbol{\Phi}^{(0)}(t_i,\tau_2)\right)^{\mathrm{T}}d\tau_1 d\tau_2\\ &+\int_{t_{i-1}}^{t_i}\int_{t_{i-1}}^{t_i}\boldsymbol{\Phi}^{(0)}(t_i,\tau_1)\boldsymbol{B}(\tau_1)\boldsymbol{C}_{\boldsymbol{u}^{\mathrm{I}}\boldsymbol{u}^{\mathrm{I}}}(\tau_1,\tau_2)\boldsymbol{B}^{\mathrm{T}}(\tau_2)\left(\boldsymbol{\Phi}^{(0)}(t_i,\tau_2)\right)^{\mathrm{T}}d\tau_1 d\tau_2\end{aligned} \tag{49}$$

Thus, only the calculations related to the integration from t_i-1 to t_i are required through (49). Afterwards, the linearization can be updated, by the CMLM, as:

$$\boldsymbol{N}^{(1)}{}_i = \left(\boldsymbol{C}_{\boldsymbol{x}^{\mathrm{I}}\boldsymbol{x}^{\mathrm{I}}}{}^{(0)}(t_i,t_i)\right)^{-1}\boldsymbol{\rho}_{\mathrm{s}}{}^{(0)}\left(f^{\mathrm{I}},\boldsymbol{x}^{\mathrm{I}}\right)\cdot\mathrm{diag}\left\{\left(f^{\mathrm{R}}x_n{}^{\mathrm{R}}\right)^{(0)}\right\} \tag{50}$$

And the state transition matrix can also be updated by the latest $\boldsymbol{N}$, repeat the calculation (47)-(50), until $\boldsymbol{N}$ satisfies the following criterion:

$$\left|\boldsymbol{N}^{(j)}{}_i - \boldsymbol{N}^{(j-1)}{}_i\right| < e^* \tag{51}$$

Finally, the optimal approximate linear equation and the corresponding covariance matrix, at time t_i, are obtained.

$$\begin{aligned}\boldsymbol{N}^*{}_i &= \boldsymbol{N}^{(j)}{}_{i+1}\\ \boldsymbol{C}_{\boldsymbol{x}^{\mathrm{I}}\boldsymbol{x}^{\mathrm{I}}}(t_i,t_i) &= \boldsymbol{C}_{\boldsymbol{x}^{\mathrm{I}}\boldsymbol{x}^{\mathrm{I}}}{}^{(j)}(t_i,t_i)\end{aligned} \tag{52}$$

Through applying the above iterative process, from initial time t_0 to the final time T, the uncertainty propagation problem can be solved completely. And the flowchart of the whole process is presented in Fig. 4, meanwhile, the main process is illustrated as follow:

Step 1 Provide the initial conditions: $\boldsymbol{x}^{\mathrm{M}}(t_0)$, $\boldsymbol{x}^{\mathrm{R}}(t_0)$, $\boldsymbol{C}(t_0, t_0)$. Define the time span and other options of ODE numerical method. Define an initial value of state matrix of approximate linear system $\boldsymbol{N}_0{}^*$. Define the order of Chebyshev polynomial n, and according the dimension of the dynamic

problem, determine the number of interpolation points m for the construction of Chebyshev-polynomial approximation. Let $i = 0$;

Step 2 Refer to the process established in Section 3.1. Take m sets of interpolation points of $\boldsymbol{x}^{\mathrm{I}}(t_0)$ in IM domain, according to the initial conditions, for the construction of Chebyshev polynomial. Then calculate the response to these points at the next time t_1 through the numerical ODE method;

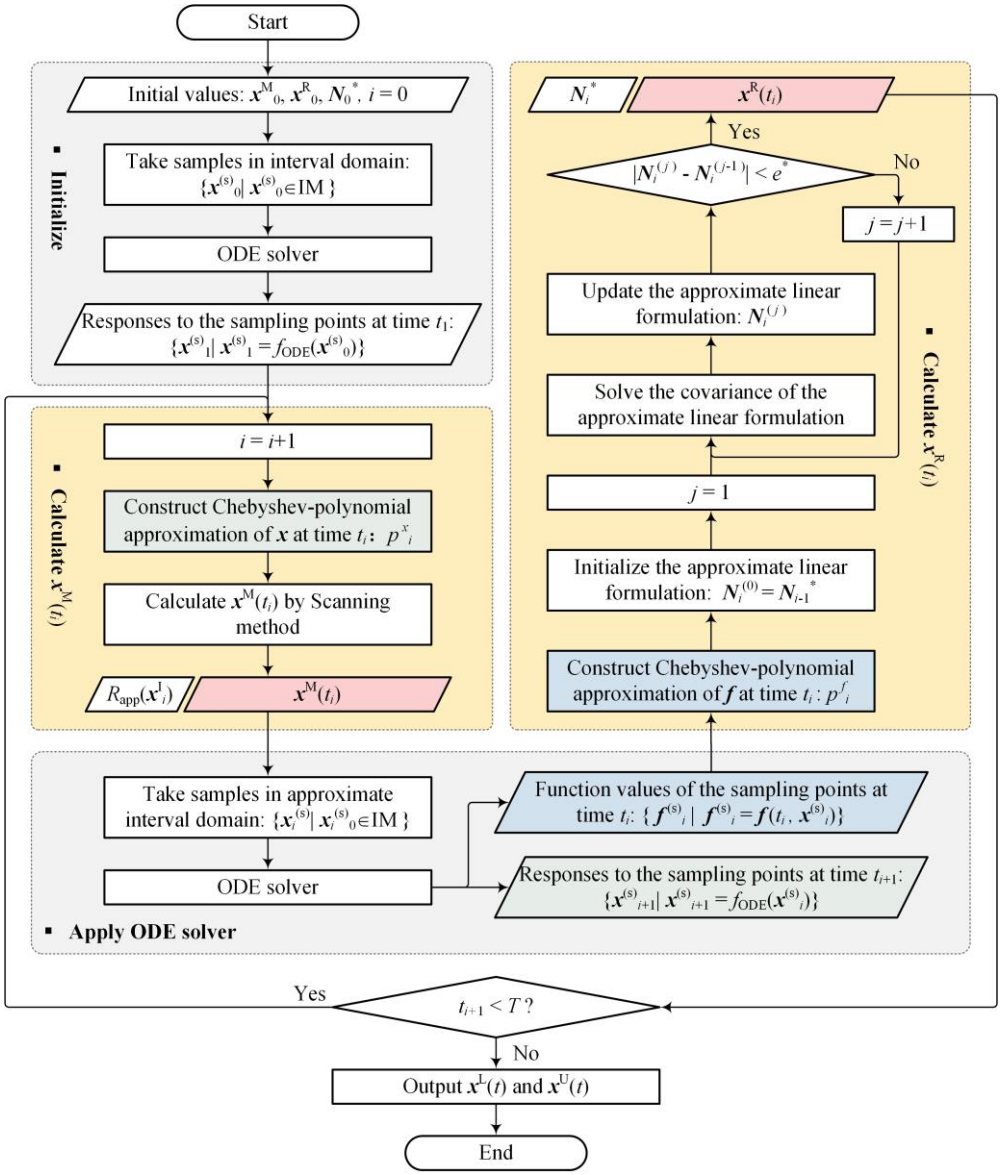

Fig. 4 The process to solve uncertainty propagation of nonlinear dynamics based on the CMLM

Step 3 Let $i = i + 1$. Construct Chebyshev-polynomial approximation of the nonlinear function between $\boldsymbol{x}(t_{i-1})$ and $\boldsymbol{x}(t_i)$, then, scan to find $\boldsymbol{x}^{\mathrm{M}}(t_i)$. Meanwhile, according to the sampling points, evaluate an approximated radius $R_{\mathrm{app}}(\boldsymbol{x}^{\mathrm{I}}(t_i))$ as:

$$R_{\text{app}}(\boldsymbol{x}^{\text{I}}(t_i)) = \alpha\left(\frac{\max\left(\boldsymbol{x}^{(\text{s})}(t_i)\right) - \min\left(\boldsymbol{x}^{(\text{s})}(t_i)\right)}{2}\right)$$

where α is an amplification coefficient, which is in range [2, 5], to ensure the domain to construct Chebyshev-polynomial approximation, for the following step, totally envelope the exact domain of $\boldsymbol{x}(t_i)$;

Step 4 Refer to the process established in Section 3.1. Take m sets of interpolation points of $\boldsymbol{x}^{\text{I}}(t_i)$ in IM domain, according to the approximated domain obtained in the Step 3. Then calculate the responses to the sampling points at next time t_{i+1} through the numerical ODE method. Meanwhile, due to the property of ODE numerical method, the value of nonlinear function $\boldsymbol{f}(\cdot)$ at $\boldsymbol{x}^{(\text{s})}(t_i)$ can also be obtained simultaneously;

Step 5 Construct Chebyshev-polynomial approximation of the nonlinear function between $\boldsymbol{x}(t_i)$ and $\boldsymbol{f}(\boldsymbol{x}(t_i))$. Initialize the approximate linear system from t_{i-1} to t_i, and let $\boldsymbol{N}_i^{(0)} = \boldsymbol{N}_{i-1}^{*}$. Let $j = 1$;

Step 6 Carry out the calculation (47)-(50), however all the calculations of nonlinear function are replaced by the Chebyshev-polynomial approximation constructed in step 5. If $\boldsymbol{N}_i^{(j)}$ satisfies the criterion (51) go to the next step, else let $j = j + 1$ and repeat Step 6;

Step 7 If $t_i < T$, go to the step 3, else output $\boldsymbol{x}^{\text{L}}(t)$ and $\boldsymbol{x}^{\text{U}}(t)$ at every discrete time points.

The time step of ODE numerical method should be determined according to the simulation precision of the middle-point function. In other words, the time step equals to the one of the simulations of the nominal trajectory.

For the Step 3, there exists an alternative approach to calculate the middle-point function. For the systems with small uncertainties, the middle-point function can be approximated by the nominal trajectory. Therefore, the nominal trajectory can be calculated previously. And in the iteration, the calculation of middle-point can be replaced by letting the middle-point $\boldsymbol{x}^{\text{M}}(t_i)$ equal to the nominal value at t_i.

4. Tests and discussions

4.1. Numerical tests

Two numerical tests are set to demonstrate the effectiveness of the proposed method. The Runge–Kutta method (RKM) is employed as the ODE solver. The order of Chebyshev polynomials for the

approximation is defined as 2. In each example, the problem is solved through the CMLM, as well as 100, 500, 1000 and 10000 MC analyses, respectively. The results of 10000 MC analyses are regarded as a standard to exam the precision of the other analyses. And the approach to achieve MC simulation for interval process is described in detail in the literature [30].

4.1.1. Duffing oscillator analysis

At first a single-degree-of-freedom duffing oscillator system is considered as:

$$m^{\mathrm{I}}\ddot{x}^{\mathrm{I}}(t)+c^{\mathrm{I}}\dot{x}^{\mathrm{I}}(t)+k^{\mathrm{I}}\left(x^{\mathrm{I}}(t)+\varepsilon\left(x^{\mathrm{I}}(t)\right)^{3}\right)=u(t) \tag{53}$$

Under an uncertain excitation $u^{\mathrm{I}}(t)$ described as an interval process, the problem can be expressed as:

$$\begin{aligned}\dot{x}_1^{\mathrm{I}}(t)&=\frac{1}{m}\left(-cx_1^{\mathrm{I}}(t)-k\left(x_2^{\mathrm{I}}(t)+\varepsilon\left(x_2^{\mathrm{I}}(t)\right)^{3}\right)\right)+\frac{1}{m}u^{\mathrm{I}}(t)\\ \dot{x}_2^{\mathrm{I}}(t)&=x_1^{\mathrm{I}}(t)\end{aligned} \tag{54}$$

where the initial condition is given as $[x_1(t_0), x_2(t_0)]^{\mathrm{T}} = [0, 0]^{\mathrm{T}}$; m, c and k equal to 1, 0.5π and $4\pi^2$, respectively; ε equals to 1. Moreover, the middle-point function, radius function and correlation-coefficient function of $u^{\mathrm{I}}(t)$ are given as:

$$\begin{aligned}u^{\mathrm{M}}(t)&=10\\ u^{\mathrm{R}}(t)&=1\\ \rho_{\omega^{\mathrm{I}}}(\tau)&=\delta(\tau)\end{aligned} \tag{55}$$

The problem is solved in the time period of 0-5, and the time step of RKM is 0.025s. The lower and upper bounds obtained by MCLM and 10000-MC-analyses samples are shown in Fig. 5. Obviously, the samples are tightly enveloped by the lower and upper bounds.

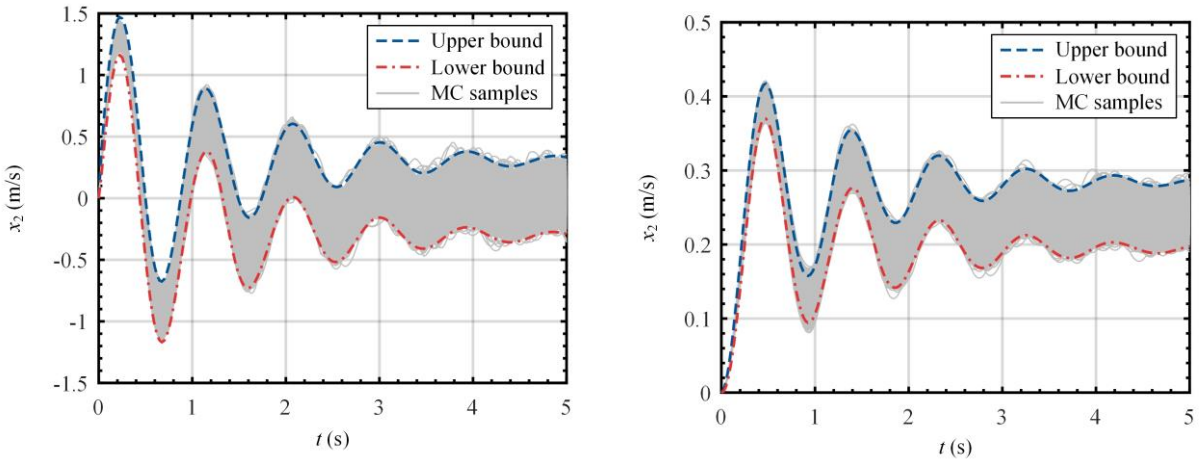

(a) x_1 (b) x_2

Fig. 5 The lower-and-upper bounds and 10000-MC-analyses samples of x_1 and x_2

For a further analysis of precision, 20 discrete time points, at 0.25s intervals, are selected, and the value of radius function at these points yielded by the CMLM, 100, 500 and 1000 MC analyses are compared to the ones of 10000 MC analyses. The sum of squares of error can be calculated as:

$$e^2 = \sum_{i=1}^{N} \left(x^{\mathrm{R}}(t_i) - x^{\mathrm{R}}{}_{\mathrm{std}}(t_i) \right)^2 \tag{56}$$

where N, the number of discrete time points, equals to 20 in the example; $x^{\mathrm{R}}{}_{\mathrm{std}}$ represents a standard solution, and it is the results of 10000 MC analyses. Then the CMLM, as well as 100, 500 and 1000 MC analyses are respectively repeated 50 times. Subsequently, the values of e^2 of x_2 obtained by the above methods at all run-times are represented as a boxplot in Fig. 6. The error of the CMLM seems to be comparable to 100 MC analyses, and be larger than the other analyses. However, actually, when $t > 1.25$s, the error of the CMLM drops significantly, as shown in (b) of Fig. 6. The error of the CMLM at the time-points, which are larger than 1.25s, is much smaller than that of 1000 MC simulation. Meanwhile, the MCLM presents a greater robustness due to the analytical solution of covariance. In brief, the CMLM performances well in precision and robustness expect for a slight error in a very short initial stage.

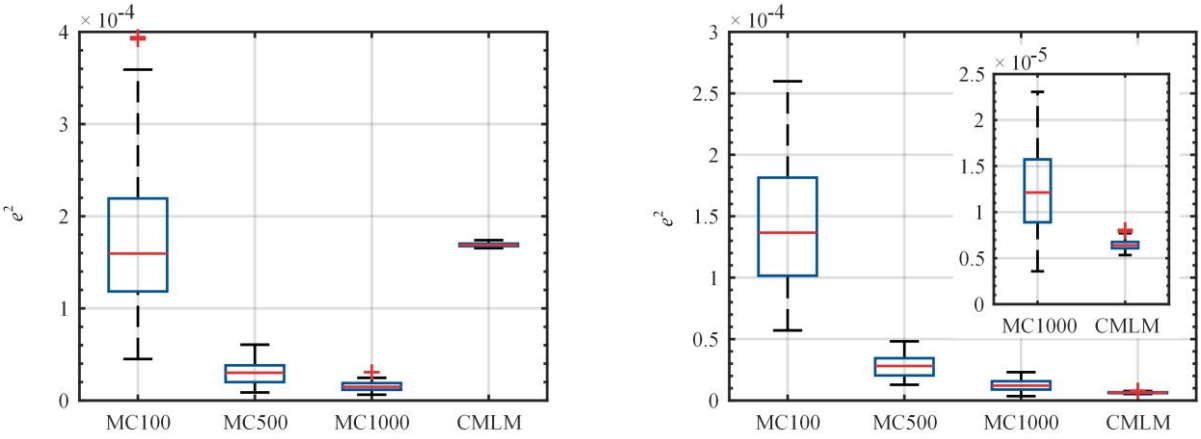

(a) $0 \leq t \leq 5$ (b) $1.25 \leq t \leq 5$

Fig. 6 The boxplot of e^2 of x_2 after a 50-time test

Finally, the precision and efficiency are concluded in Table 1. The CTPM are applied to construct Chebyshev-polynomial approximation, therefor, for the 2-dimensional problem, 9 interpolation points are required, accordingly, the times to apply ODE solver, N_{ODE}, is 9. The CMLM can achieve higher accuracy with much less computational cost than no less than 1000 MC analyses.

Table 1 Precision and efficiency of different methods in calculating x_2 for a duffing oscillator

Method	Mean of relative error to MC10000		N_{ODE}
	$0 \le t \le 5$	$1.25 \le t \le 5$	
MC100	5.21%	5.84%	100
MC500	2.47%	2.46%	500
MC1000	1.66%	1.62%	1000
CMLM	3.91%	**0.83%**	**9**

4.1.2. Vehicle ride analysis

In the second example, a two-degree-of-freedom quarter-car model[20,18,23] is analyzed, as shown in Fig. 7.

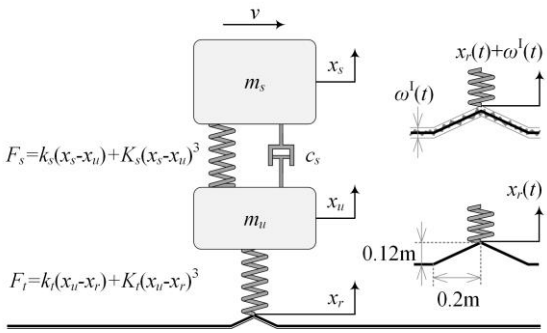

Fig. 7 The schematic of a quarter-car model with two-degree-of-freedom and the roughness of the road

$$\begin{cases} \dot{x}_s = v_s \\ \dot{x}_u = v_u \\ \dot{v}_s = -\dfrac{1}{m_s}\left(c_s\left(v_s - v_u\right) + k_s\left(x_s - x_u\right) + K_s\left(x_s - x_u\right)^3\right) \\ \dot{v}_u = \dfrac{1}{m_u}\left(c_s\left(v_s - v_u\right) + k_s\left(x_s - x_u\right) + K_s\left(x_s - x_u\right)^3 + k_t\left(x_r - x_u\right) + K_t\left(x_r - x_u\right)^3\right) \end{cases} \tag{57}$$

where the initial condition is given as $[x_s(t_0), x_u(t_0), v_s(t_0), v_u(t_0)]^T = [0, 0, 0, 0]^T$; m_s and m_u equal to 400 and 600, respectively; c_s, k_s and k_t equal to 1000, 1.5×10^4 and 2×10^5, respectively; K_s and K_u equal to 1.5×10^6 and 2×10^7, respectively.

It is supposed that the vehicle drives through a standard triangular road block with a speed of v = 10m/s, x_r can then be given by

$$x_r = \begin{cases} 6t & 0,, \ t < 0.02 \\ 0.24 - 6t & 0.02,, \ t < 0.04 \\ 0 & t..0.04 \end{cases} \tag{58}$$

Then the standard triangular road block is supposed to be rough, and under the interval process model,

due to an additional roughness $\omega^{\mathrm{I}}(\mathrm{t})$, $x_{\mathrm{r}}(t)$ is transformed into an interval process $x_{\mathrm{r}}^{\mathrm{I}}(t)$ as

$$x_r^{\mathrm{I}}(t)=x_r(t)+\omega^{\mathrm{I}}(t) \tag{59}$$

where $\omega^{\mathrm{I}}(\mathrm{t})$ is defined as the following stationary interval process, that

$$\begin{aligned}&\omega^{\mathrm{M}}(t)=0\\&\omega^{\mathrm{R}}(t)=3\times10^{-3}\\&\rho_{\omega^{\mathrm{I}}}(\tau)=\delta(\tau)\end{aligned} \tag{60}$$

Afterwards, through neglecting the effect of $\omega^{\mathrm{I}}(\mathrm{t})$ to the three-order term, the nonlinear dynamics with time-varying interval uncertainties problem can be defined as

$$\begin{cases}\dot{x}_s^{\mathrm{I}}(t)=v_s^{\mathrm{I}}(t)\\\dot{x}_u^{\mathrm{I}}(t)=v_u^{\mathrm{I}}(t)\\\dot{v}_s^{\mathrm{I}}(t)=f_s\\\dot{v}_u^{\mathrm{I}}(t)=f_u+\dfrac{k_t}{m_u}\omega^{\mathrm{I}}(t)\end{cases} \tag{61}$$

where f_s and f_u denote the nonlinear functions of v_s and v_u in (57).

The problem is solved in the time period of 0-1s, and the time step of RKM is 2×10^{-3}s. The lower and upper bounds obtained by MCLM and 10000-MC-analyses samples are shown in Fig. 8. Similarly, 20 discrete time points, at 0.05s intervals, are also selected. And by comparing to the results of 10000 MC analyses, the sum of squares of error of x_s^{R} obtained by the CMLM, MC simulation of 100, 500 and 1000 times are calculated. The results of a 50-time reptation are represented as a boxplot Fig. 9. With the comparation to 1000 MC analyses, the MCLM has a comparable but slightly larger error from 0s to 1s as shown in (a) of Fig. 9. However, when $0.35 \le t \le 1$, the MCLM achieves a higher precision than other approaches as shown in (b) of Fig. 9.

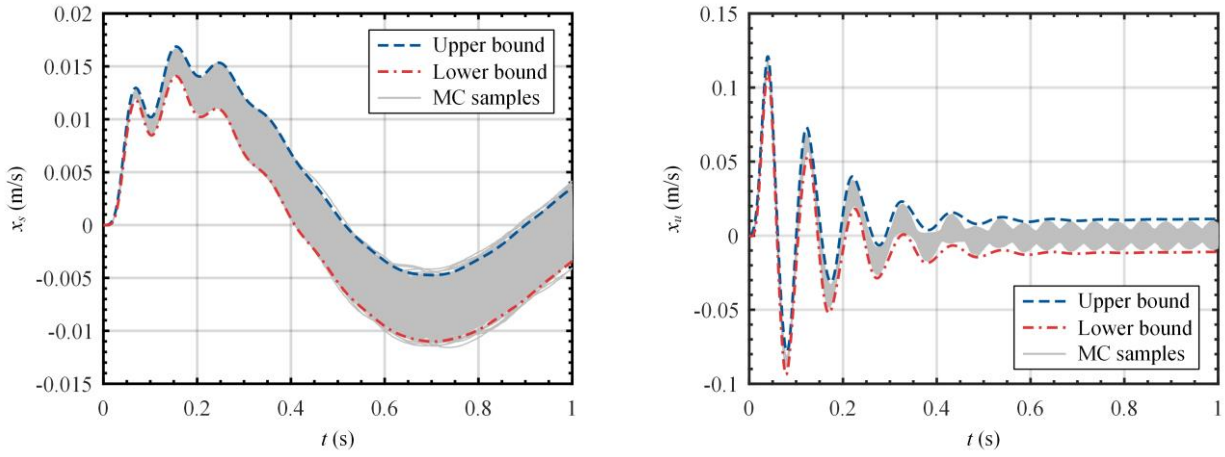

(a) x_s (b) x_u

Fig. 8 The lower-and-upper bounds and 10000-MC-analyses samples of x_s and x_u

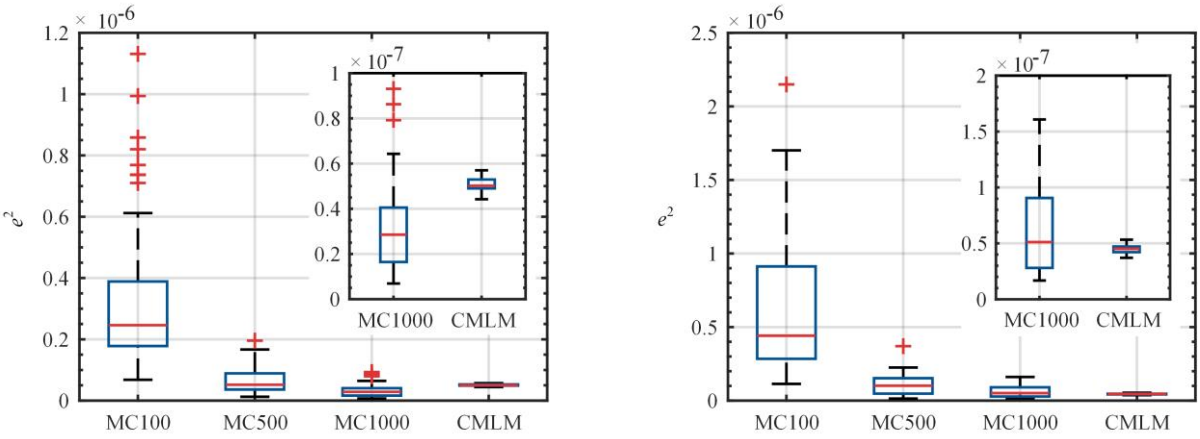

(a) $0 \le t \le 1$ (b) $0.14 \le t \le 1$

Fig. 9 The boxplot of e^2 of x_r after a 50-time test

At last, the details of precision and efficiency are listed in Table 2. The CTPM is selected to construct Chebyshev-polynomial approximation, thus, 81 times numerical solution of ODE is required due to 81 necessary interpolation points. From the comparation, the CMLM achieve comparable precision to 1000 MC analyses with a much higher efficiency.

Table 2 Precision and efficiency of different methods in calculating x_s for a vehicle ride analysis

Method	Mean of relative error to MC10000		N_{ODE}
	$0 \le t \le 1$	$0.14 \le t \le 1$	
MC100	5.08%	5.61%	100
MC500	2.27%	2.72%	500
MC1000	1.66%	1.64%	1000
CMLM	4.41%	**1.46%**	**81**

4.2. Application in uncertainty propagation of LV ascent trajectory

The concept of LV-flight-dynamic model is shown in Fig. 10, and corresponding three-degree-of-freedom dynamic equations can be expressed in a vector form as (62), which describes the motion of the center of mass of a LV.

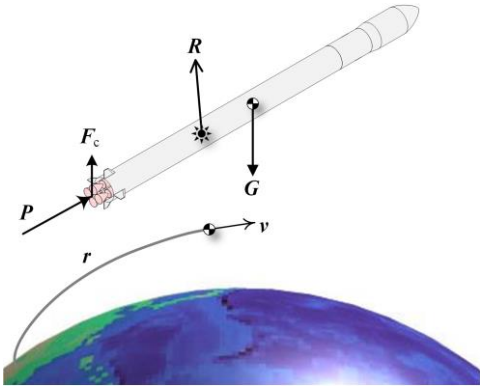

Fig. 10 The concept of LV-flight-dynamic model

$$\begin{cases} \dot{\boldsymbol{v}} = \dfrac{1}{m}\left(\boldsymbol{G} + \boldsymbol{R} + \boldsymbol{P} + \boldsymbol{F}_{\mathrm{c}}\right) \\ \dot{\boldsymbol{r}} = \boldsymbol{v} \end{cases} \tag{62}$$

where, $\boldsymbol{v}$ (= $[v_x, v_y, v_z]^{\mathrm{T}}$) is the velocity vector of the LV; $\boldsymbol{r}$ (= $[r_x, r_y, r_z]^{\mathrm{T}}$) is the position vector of the center of mass of the LV; m is the mass of the LV; $\boldsymbol{G}$, $\boldsymbol{R}$, $\boldsymbol{P}$, and $\boldsymbol{F}_{\mathrm{c}}$ are, respectively, gravity, aerodynamic force, propulsion, and control force on the LV. The detailed expansion of the model is illustrated in Appendix C.

In practical engineering, the values of the above forces cannot be obtained analytically, and are always provided in the form of complex discrete tables. Therefore, the dynamic model is usually too complex to be modified arbitrarily and the calculation of LV trajectory is generally regarded as a black-box problem.

4.2.1. Uncertainty propagation problems

Consider a three-stage LV, and the basic parameters of the LV are provided in Table 3. Meanwhile, the parameters of the flight conditions are listed in Table 4. The flight-program angle, the control program formulated to make the LV fly according to a certain flight trajectory, is given as (63). Based on the above parameters, the baseline trajectory is simulated as shown in Fig. 11.

$$\varphi_{\mathrm{PR}}(t) = \begin{cases} \dfrac{\pi}{2} & 0\mathrm{s} \le t < 10\mathrm{s} \\ \dfrac{\pi}{2} + \left(\dfrac{\pi}{2} - \dfrac{\pi}{60}\right)\left(\left(\dfrac{t-10}{150}\right)^2 - 2\left(\dfrac{t-10}{150}\right)\right) & 10\mathrm{s} \le t < 160\mathrm{s} \\ \dfrac{\pi}{60} & t > 160\mathrm{s} \end{cases} \tag{63}$$

Table 3 Basic parameters of the LV

Parameter	Symbol	Unit	Value	Parameter	Symbol	Unit	Value
Total mass	m	t	35.40	**Substage 2**			
Total length	L	m	18.26	Substage mass	m_2	t	7.05
Maximum diameter	D	m	1.67	Propellent mass	m_{p2}	t	270
Substage 1				Propulsion	P_2	kN	270
Substage mass	m_1	t	22.68	working time	t_2	s	65.20
Propellent mass	m_{p1}	t	20.80	**Substage 3**			
Propulsion	P_1	kN	912	Substage mass	m_3	t	3.65
working time	t_1	s	61.60	Propellent mass	m_{p3}	t	3.32
-	-	-	-	Propulsion	P_3	kN	155
-	-	-	-	working time	t_3	s	59.6

Table 4 Parameters of the flight conditions

Symbol	Unit	Value	Symbol	Unit	Value
Launch point			**Earth**		
R_{0x}	m	0	a_e	m	6378145
R_{0y}	m	6378145	b_e	m	6356760
R_{0z}	m	0	ω_e	m/s	7.292×10^{-5}
Gravity			ω_{ex}	m/s	7.292×10^{-5}
μ	m^3/s^2	3.986×10^{14}	ω_{ey}	m/s	0
J	-	1.624×10^{-3}	ω_{ez}	m/s	0
Aerodynamic coefficients			-	-	-
C_x	-	0.2	-	-	-
C_y^{α}	1/°	0.07	-	-	-

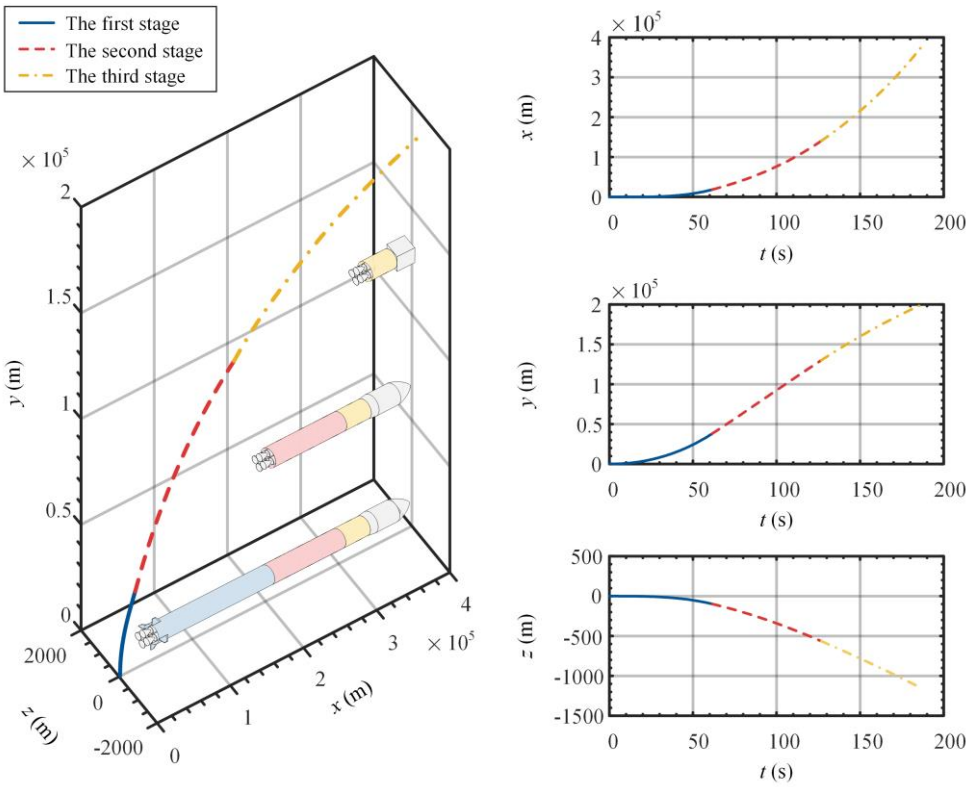

Fig. 11 The baseline trajectory of the LV

The actual flight of the LV is usually affected by various uncertainties [37-39], the most common one is the variation of atmosphere environment. Especially, the impact is obvious to the-first-stage flight, due to a dense atmosphere condition at this stage, as shown in Fig. 12.

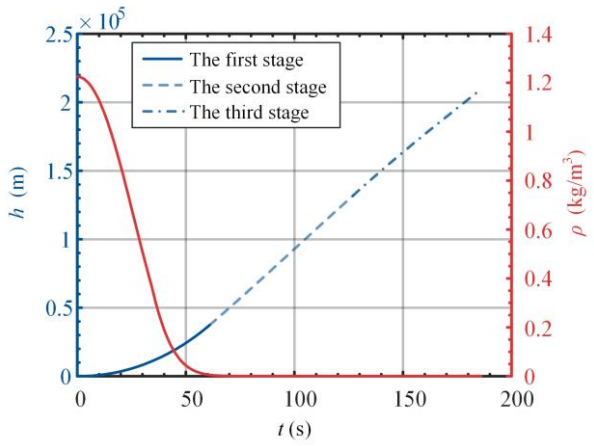

Fig. 12 Comparison for the variation of flight height and atmospheric density

Therefore, it is necessary to quantify the influence of the atmosphere uncertainty, however, it is obviously a time-varying uncertainty. And, to obtain the precise information of it, a great amount of cost in both experiment and time are generally required. At an earlier phase of design, only the worst condition needs to considered, thus the interval process is an extremely proper model to describe the uncertainty. Accordingly, the problem of the-first-stage flight is established as a time-varying interval uncertainty propagation problem, which is illustrated in detail as follow.

Let $\boldsymbol{x} = [\boldsymbol{v}^{\mathrm{T}}, \boldsymbol{r}^{\mathrm{T}}]^{\mathrm{T}}$, the dynamic model (62) can be expressed as:

$$\dot{\boldsymbol{x}} = \boldsymbol{f}(\boldsymbol{x}, t) \tag{64}$$

where $\boldsymbol{f}(\cdot)$ represents the nonlinear-function vector in (62), and t is the flight time.

Problem 1: The wind will change the flight state of the LV through additional aerodynamic force, in other words it will cause additional acceleration. Due to that the direction of wind is random, the additional acceleration may occur probably in all three degrees of freedom. Therefore, the problem is formulated as:

$$\dot{\boldsymbol{x}}^{\mathrm{I}}(t) = \boldsymbol{f}\left(\boldsymbol{x}^{\mathrm{I}}(t), t\right) + \left[\omega_x^{\mathrm{I}}(t), \omega_y^{\mathrm{I}}(t), \omega_z^{\mathrm{I}}(t), 0, 0, 0\right]^{\mathrm{T}} \tag{65}$$

where $\omega_x^{\mathrm{I}}(\mathrm{t})$, $\omega_y^{\mathrm{I}}(\mathrm{t})$, and $\omega_z^{\mathrm{I}}(\mathrm{t})$ are additional accelerations described by stationary interval processes, which is similar to the model of wind in probabilistic method. Then middle-point function, radius

function and the cross-covariance matrix function of $\boldsymbol{\omega}^{\mathrm{I}}(\mathrm{t})$ are respectively defined as

$$\begin{aligned}
&\omega_x^{\mathrm{M}}(t)=\omega_x^{\mathrm{M}}(t)=\omega_x^{\mathrm{M}}(t)=0\\
&\omega_x^{\mathrm{R}}(t)=\omega_x^{\mathrm{R}}(t)=\omega_x^{\mathrm{R}}(t)=2\left(\mathrm{m/s^2}\right)\\
&\boldsymbol{C}_{\omega^{\mathrm{I}}\omega^{\mathrm{I}}}(\tau)=\begin{bmatrix}\delta(\tau) & 0 & 0\\ 0 & \delta(\tau) & 0\\ 0 & 0 & \delta(\tau)\end{bmatrix}
\end{aligned} \tag{66}$$

Problem 2: After that, the uncertainty propagation of the following two-stage flight should to be considered. At this moment, according to Fig. 12, the LV has left the area with dense atmosphere, thus there is few obvious external time-varying uncertainties. The flight is mainly impacted by uncertain initial conditions left by the first stage. Thus, the uncertainty propagation of the last two stages can be expressed as:

$$\begin{cases}\dot{\boldsymbol{x}}^{\mathrm{I}}(t)=\boldsymbol{f}\left(\boldsymbol{x}^{\mathrm{I}}(t),t\right)\\ \boldsymbol{x}^{\mathrm{I}}(t_0)=\boldsymbol{x}_0^{\mathrm{I}}\end{cases} \tag{67}$$

In conclusion, the uncertainty propagation of LV trajectory is defined, which is divided into two sub-problems, one is a problem with time-varying uncertainties of the first stage formulated as (65), and the other is a problem with correlated initial uncertainties of the second and third stage formulated as (67).

4.2.2. Results and discussions

Firstly, the Problem 1 is solved through the CMLM, in the time period of 0-60s. The RKM is applied as the solver, and the time step is 0.5s. The order of Chebyshev polynomials for the approximation is defined as 2. The lower and upper bounds obtained by MCLM with comparation to 10000-MC-analyses samples are shown in Fig. 13.

Then 12 discrete points, at 5s intervals, are selected from 0s to 60s. At these points, the e^2 of v_z and z obtained by the CMLM, 100, 500 and 1000 MC analyses are calculated, respectively. The standard solution in this case is still the results of 10000 MC analyses. Afterwards, the values of e^2 after a 50-time test are represented as boxplot in Fig. 14. It is shown that the CMLM performance a better robustness meanwhile provides a result with comparable precision to 1000 MC analyses.

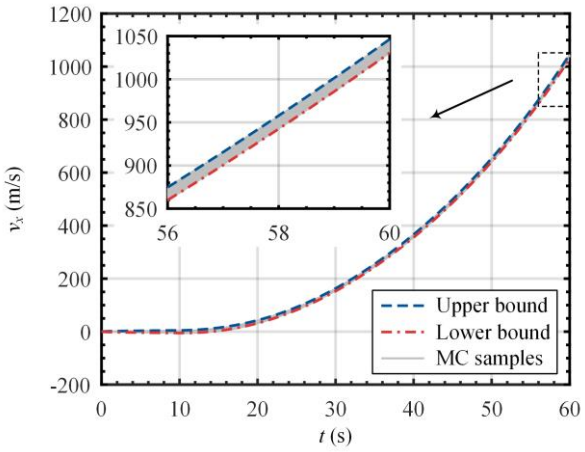

(a) v_x

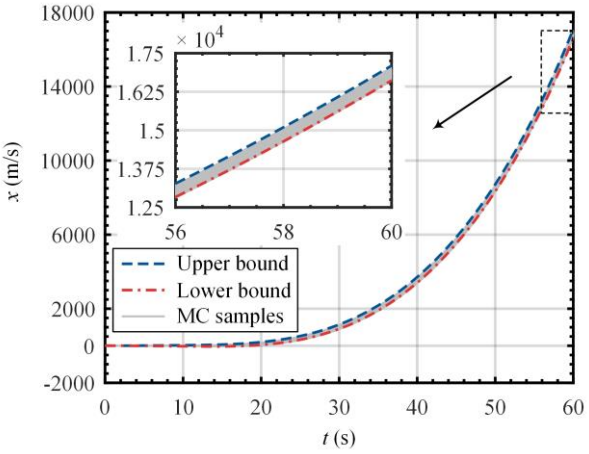

(b) x

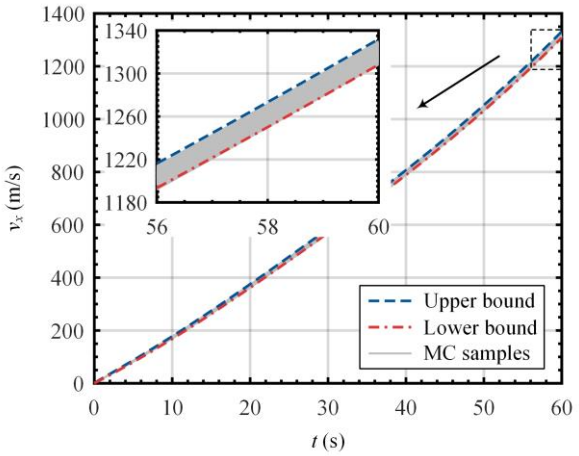

(c) v_y

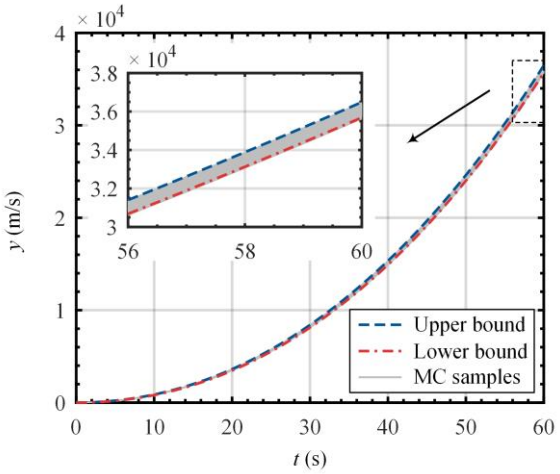

(d) y

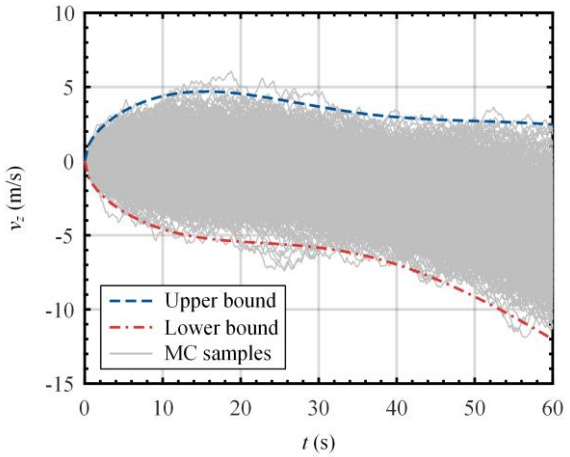

(e) v_z

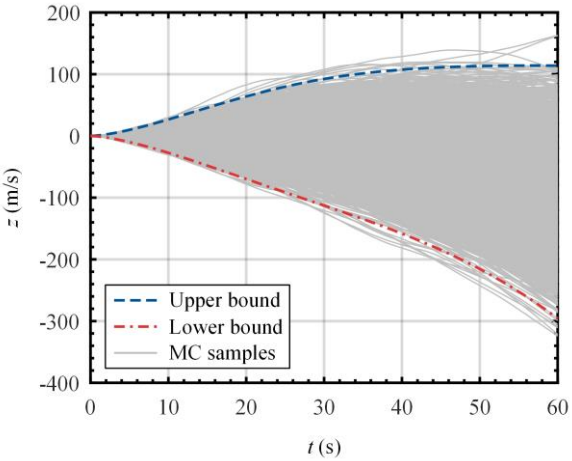

(f) z

Fig. 13 The lower-and-upper bounds and 10000-MC-analyses samples of the first-stage flight

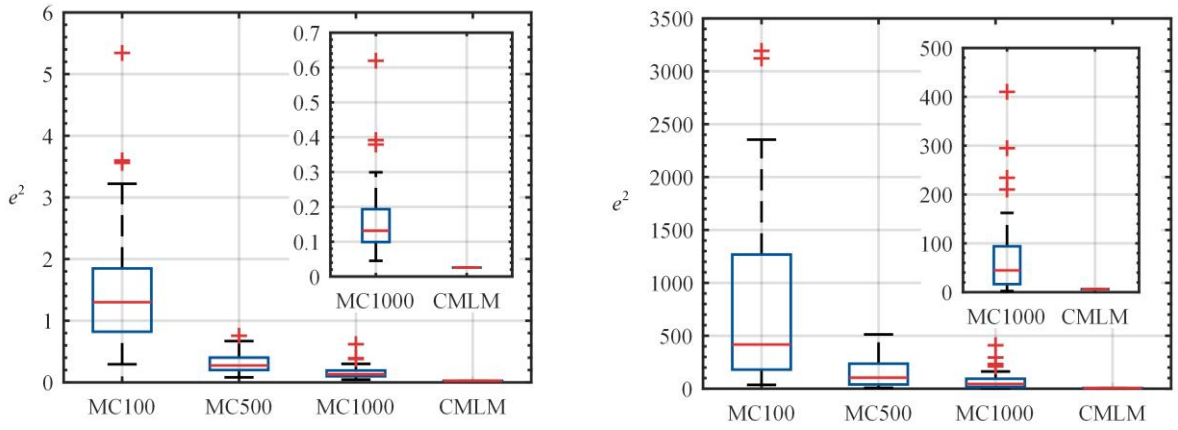

(a) v_z (b) z

Fig. 14 The boxplot of e^2 of v_z and z after a 50-time test

Finally, the precision and efficiency are concluded in Table 6. For a 6-dimentional problem, the CCM is chose to construct Chebyshev-polynomial approximation. Therefore, at least 56 interpolation points are required, while the minimum times of numerical solution of ODE is 56. It is shown that, MCLM achieves a higher precision than 1000 MC analyses in v_y, v_z, y and z with a considerably smaller computational cost. Thus, it can be concluded that the MCLM performances well in precision, efficiency and robustness for a practical LV trajectory problem under time-varying uncertainties.

Table 5 Precision and efficiency of different methods in calculating v_z *and* z for the first-stage flight

Method	Mean of relative error to MC10000						N_{ODE}
	v_x	x	v_y	y	v_z	z	
MC100	5.94%	6.25%	5.93%	5.99%	5.27%	5.44%	100
MC500	2.69%	2.88%	2.44%	2.37%	2.51%	2.67%	500
MC1000	1.69%	1.57%	1.60%	1.70%	1.69%	1.57%	1000
CMLM	2.13%	2.80%	**0.68%**	**0.88%**	**0.63%**	**0.39%**	**56**

After the uncertainty propagation of the first-stage flight, a correlated uncertain domain of the final state is caused. The values of middle-point and radius are listed in Table 6, meanwhile, the correlation-coefficient matrix is expressed as follow:

$$\boldsymbol{\rho} = \begin{array}{c} \begin{matrix} v_x & v_y & v_z & x & y & z \end{matrix} \\ \begin{bmatrix} 1 & 0.21 & 0 & 0.68 & 0.18 & 0 \\ & 1 & 0 & 0.24 & 0.89 & 0 \\ & & 1 & 0 & 0 & 0.64 \\ & & & 1 & 0.24 & 0 \\ & & & & 1 & 0 \\ & & & & & 1 \end{bmatrix} \end{array} \begin{matrix} v_x \\ v_y \\ v_z \\ x \\ y \\ z \end{matrix}$$

Table 6 Values of middle-point and radius for the final state after the first-stage flight

Parameter	v_x	v_y	v_z	x	y	z
Unit	m/s	m/s	m/s	m	m	m
Middle-point value	1061.44	1349.66	-4.86	17382.59	36754.38	-93.27
Radius	7.98	12.34	7.32	240.35	413.06	207.33

Under the above initial-value uncertainties, the Problem 2 can also be solved through the CMLM, and the results are shown in Fig. 15. The problem is solved in the time period of 60s-185s, and the RKM is still employed as the solver. The order of Chebyshev polynomials for the approximation is also defined as 2. The lower and upper bounds of v_z and z obtained by the CMLM with comparation to 10000-time-MC samples are shown in Fig. 15. Then 25 discrete points, at 5s intervals, are selected from 60s to 185s. At these points, compared with 10000 MC analyses, the e^2 of v_z and z obtained by the CMLM and 100, 500 and 1000 MC analyses are represented as boxplot in Fig. 16, and the precision and efficiency are concluded in Table 7. It is shown that the CMLM performance a better in precision and robustness than 1000 MC analyses with only 56 times of calculation of original functions.

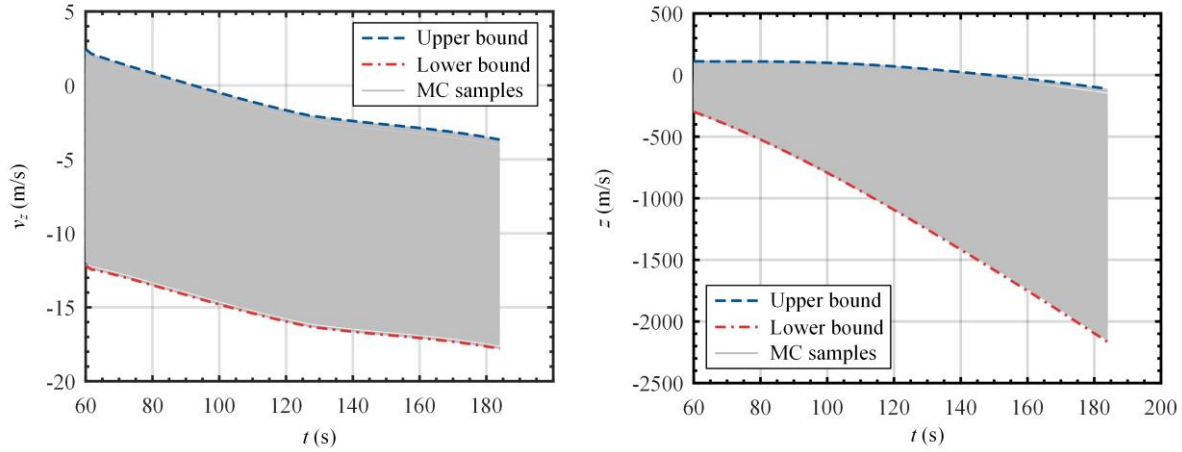

(a) v_z (b) z

Fig. 15 The lower-and-upper bounds and 10000-MC-analyses samples of v_z and z of the second and third flight

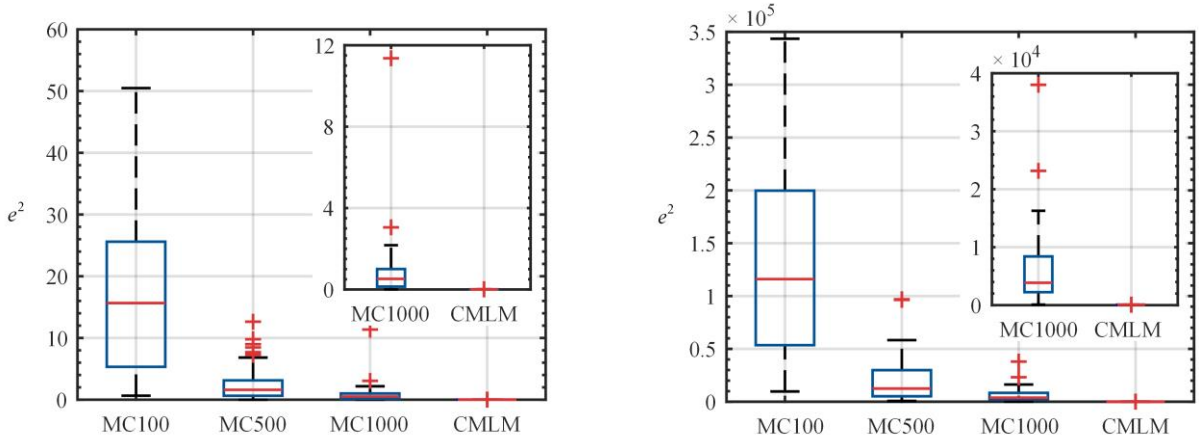

(a) x (b)y

Fig. 16 The boxplot of e^2 of v_z and z after a 50-time test for the second-and-third-stage flight

Table 7 Precision and efficiency of different methods in calculating v_z *and* z for the second-and-third-stage flight

Method	Mean of relative error to MC10000						N_{ODE}
	v_x	x	v_y	y	v_z	z	
MC100	3.18%	2.21%	1.27%	0.75%	2.18%	1.80%	100
MC500	1.50%	1.02%	0.65%	0.38%	0.80%	0.66%	500
MC1000	1.02%	0.80%	0.38%	0.25%	0.43%	0.35%	1000
CMLM	**0.46%**	**0.26%**	**0.32%**	**0.09%**	**0.05%**	**0.07%**	**56**

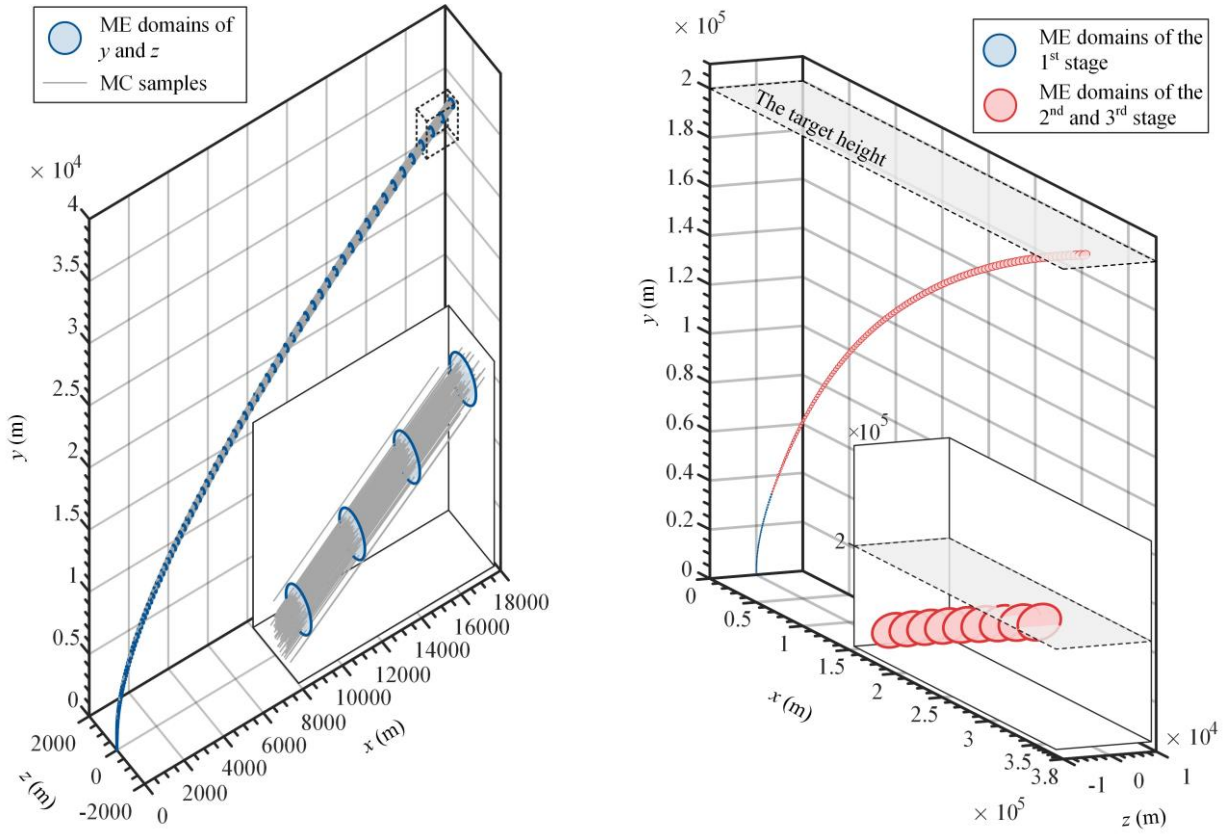

(a) Uncertainty propagation of the first stage flight (b) Uncertainty propagation of the second-and-third stage flight

Fig. 17 Uncertainty propagation of the LV ascent trajectory

Eventually, through solving Problem 1 and Problem 2, the uncertainty propagation of the whole trajectory is obtained, as shown in Fig. 17. The results demonstrate the effectiveness of the proposed CMLM in solving practical engineering nonlinear dynamics with time-varying uncertainties and correlated initial uncertainties under the interval process model.

5. Conclusion

In this work, the interval process model is applied to dynamic response evaluation of nonlinear systems, in which only upper and lower bounds of uncertainties are required rather than precise probability distributions, and autocorrelations and cross-correlations of the time-varying interval variables are quantified. In order to efficiently solve the problem of uncertainty propagation under the interval process model, a linear method is proposed called CMLM.

In the CMLM, an index to evaluate the degree of approximation of a linear formulation to a nonlinear system is represented by the uncertain-response characteristics (middle-point, radius and correlation) using the MEM. Through minimizing the index, the nonlinear system is linearized without neither calculation of derivatives nor the modification of the original system. The uncertainty propagation of linearized system can be calculated analytically. Thus, the CMLM presents the following advantages. First, it is a non-intrusive approach, which avoids the tedious modification of the state equations, thus it holds the capacity to solve black-box problems using any numerical methods for ODE problems. Meanwhile, it is a semi-analytical method and accordingly presents a greater robustness. Furthermore, to reduce computational cost during the linearization process, Chebyshev-polynomial approximation is applied to replace the original nonlinear system analysis. Therefore, the CMLM performance well in efficiency, meanwhile precision is also guaranteed.

The proposed method is tested in two numerical examples, and the results show that the MCLM has comparable precision to 1000 MC analyses and only 1%-10% times of dynamic analysis of nonlinear system is required. Meanwhile it has better robustness than MC simulation of less than 1000 analyses after a 50-time repetition test. Then the CMLM is applied to a practical LV trajectory problem with black-box dynamics. The uncertainty propagations of a three-stage-LV ascent flight under external time-varying uncertainties and correlated initial uncertainties are solved. The results show that it still maintains high precision, efficiency and robustness, therefore, the effectiveness of the CMLM

for complicated black-box problems in practical engineering is demonstrated.

Appendix A: Derivation of CMLM criterion

Through weighted sum of e_1, e_2 and e_3, a comprehensive index e can be expressed as:

$$\begin{aligned} e &= e_1 + e_2 + e_3 \cdot 2 f^{\mathrm{R}} \hat{f}^{\mathrm{R}} \\ &= \left(f^{\mathrm{M}} - \hat{f}^{\mathrm{M}} \right)^2 + \left(f^{\mathrm{R}} - \hat{f}^{\mathrm{R}} \right)^2 + \left(1 - \rho_{\mathrm{s}} \left(f^{\mathrm{I}}, \hat{f}^{\mathrm{I}} \right) \right) \cdot 2 f^{\mathrm{R}} \hat{f}^{\mathrm{R}} \\ &= \left(f^{\mathrm{M}} - \hat{f}^{\mathrm{M}} \right)^2 + \left(f^{\mathrm{R}} \right)^2 + \left(\hat{f}^{\mathrm{R}} \right)^2 - 2 \rho_{\mathrm{s}} \left(f^{\mathrm{I}}, \hat{f}^{\mathrm{I}} \right) \cdot f^{\mathrm{R}} \hat{f}^{\mathrm{R}} \end{aligned} \tag{68}$$

where the SCC ρ_{s} is defined as:

$$\rho_{\mathrm{s}} \left(x_i^{\mathrm{I}}, x_j^{\mathrm{I}} \right) = \frac{\sum_{s=1}^{N_{\mathrm{s}}} \left(x_i^{(\mathrm{s})} - x_i^{\mathrm{M}} \right) \left(x_j^{(\mathrm{s})} - x_j^{\mathrm{M}} \right)}{\sqrt{\sum_{s=1}^{N_{\mathrm{s}}} \left(x_i^{(\mathrm{s})} - x_i^{\mathrm{M}} \right)^2 \sum_{s=1}^{N_{\mathrm{s}}} \left(x_j^{(\mathrm{s})} - x_j^{\mathrm{M}} \right)^2}} = \frac{\boldsymbol{r}_i^{(\mathrm{s})\mathrm{T}} \boldsymbol{r}_j^{(\mathrm{s})}}{\sqrt{\boldsymbol{r}_i^{(\mathrm{s})\mathrm{T}} \boldsymbol{r}_i^{(\mathrm{s})}} \sqrt{\boldsymbol{r}_j^{(\mathrm{s})\mathrm{T}} \boldsymbol{r}_j^{(\mathrm{s})}}} \tag{69}$$

where x^{I}_i and x^{I}_j are two interval variables; $x_i^{(\mathrm{s})}$, $x_j^{(\mathrm{s})}$ are sampling points of x^{I}_i and x^{I}_j. Therefore, the SCC of the uncertain value of the nonlinear function and its approximate linear function can be calculated as:

$$\rho_{\mathrm{s}} \left(f^{\mathrm{I}}, \hat{f}^{\mathrm{I}} \right) = \frac{\boldsymbol{r}_f^{(\mathrm{s})\mathrm{T}} \boldsymbol{r}_{\hat{f}}^{(\mathrm{s})}}{\sqrt{\boldsymbol{r}_f^{(\mathrm{s})\mathrm{T}} \boldsymbol{r}_f^{(\mathrm{s})}} \sqrt{\boldsymbol{r}_{\hat{f}}^{(\mathrm{s})\mathrm{T}} \boldsymbol{r}_{\hat{f}}^{(\mathrm{s})}}} \tag{70}$$

where

$$\begin{aligned} \boldsymbol{r}_f^{(\mathrm{s})} &= \left(f\left(\boldsymbol{x}^{(\mathrm{s})} \right) - f^{\mathrm{M}} \right) \\ \boldsymbol{r}_{\hat{f}}^{(\mathrm{s})} &= \left(\boldsymbol{N}^{\mathrm{T}} \boldsymbol{r}^{(\mathrm{s})} + \boldsymbol{M}^{\mathrm{T}} \boldsymbol{m}^{(\mathrm{s})} - \hat{f}^{\mathrm{M}} \right)^{\mathrm{T}} = \boldsymbol{r}^{(\mathrm{s})\mathrm{T}} \boldsymbol{N} \end{aligned} \tag{71}$$

Thus

$$\rho_{\mathrm{s}} \left(f^{\mathrm{I}}, \hat{f}^{\mathrm{I}} \right) = \frac{\boldsymbol{r}_f^{(\mathrm{s})\mathrm{T}} \boldsymbol{r}^{(\mathrm{s})\mathrm{T}} \boldsymbol{N}}{\sqrt{\boldsymbol{r}_f^{(\mathrm{s})\mathrm{T}} \boldsymbol{r}_f^{(\mathrm{s})}} \sqrt{\boldsymbol{N}^{\mathrm{T}} \boldsymbol{r}^{(\mathrm{s})} \boldsymbol{r}^{(\mathrm{s})\mathrm{T}} \boldsymbol{N}}} = \frac{\boldsymbol{r}_f^{(\mathrm{s})\mathrm{T}} \cdot \left[\boldsymbol{r}_i^{(\mathrm{s})\mathrm{T}}, \cdots, \boldsymbol{r}_n^{(\mathrm{s})\mathrm{T}} \right] \cdot \boldsymbol{N}}{\sqrt{\boldsymbol{r}_f^{(\mathrm{s})\mathrm{T}} \boldsymbol{r}_f^{(\mathrm{s})}} \sqrt{\boldsymbol{N}^{\mathrm{T}} \boldsymbol{r}^{(\mathrm{s})} \boldsymbol{r}^{(\mathrm{s})\mathrm{T}} \boldsymbol{N}}} \tag{72}$$

Actually, the SCC between the uncertain value of the nonlinear function and its uncertain inputs can be calculated as:

$$\begin{aligned} \boldsymbol{\rho}_{\mathrm{s}} \left(f^{\mathrm{I}}, \boldsymbol{x}^{\mathrm{I}} \right) &= \left[\rho_{\mathrm{s}} \left(f^{\mathrm{I}}, x_1^{\mathrm{I}} \right), \cdots, \rho_{\mathrm{s}} \left(f^{\mathrm{I}}, x_n^{\mathrm{I}} \right) \right]^{\mathrm{T}} \\ \rho_{\mathrm{s}} \left(f^{\mathrm{I}}, x_i \right) &= \frac{\boldsymbol{r}_f^{(\mathrm{s})\mathrm{T}} \boldsymbol{r}_i^{(\mathrm{s})\mathrm{T}}}{\sqrt{\boldsymbol{r}_f^{(\mathrm{s})\mathrm{T}} \boldsymbol{r}_f^{(\mathrm{s})}} \sqrt{\boldsymbol{r}_i^{(\mathrm{s})} \boldsymbol{r}_i^{(\mathrm{s})\mathrm{T}}}}, i = 1, 2, \ldots, n \end{aligned} \tag{73}$$

Then substitute (73) into (72) that

$$\begin{aligned} \rho_{\mathrm{s}} \left(f^{\mathrm{I}}, \hat{f}^{\mathrm{I}} \right) &= \frac{\left[\rho_{\mathrm{s}} \left(f^{\mathrm{I}}, x_1 \right) \cdot \sqrt{\boldsymbol{r}_1^{(\mathrm{s})} \boldsymbol{r}_1^{(\mathrm{s})\mathrm{T}}}, \cdots, \rho_{\mathrm{s}} \left(f^{\mathrm{I}}, x_n \right) \cdot \sqrt{\boldsymbol{r}_n^{(\mathrm{s})} \boldsymbol{r}_n^{(\mathrm{s})\mathrm{T}}} \right] \cdot \boldsymbol{N}}{\sqrt{\boldsymbol{N}^{\mathrm{T}} \boldsymbol{r}^{(\mathrm{s})} \boldsymbol{r}^{(\mathrm{s})\mathrm{T}} \boldsymbol{N}}} \\ &= \frac{\boldsymbol{\rho}_{\mathrm{s}} \left(f^{\mathrm{I}}, \boldsymbol{x} \right)}{\sqrt{\boldsymbol{N}^{\mathrm{T}} \boldsymbol{r}^{(\mathrm{s})} \boldsymbol{r}^{(\mathrm{s})\mathrm{T}} \boldsymbol{N}}} \cdot \mathrm{diag} \left(\sqrt{\boldsymbol{r}_i^{(\mathrm{s})} \boldsymbol{r}_i^{(\mathrm{s})\mathrm{T}}} \right) \cdot \boldsymbol{N} \end{aligned} \tag{74}$$

Through the substituting (75) into (68), e can be expressed as:

$$e = \left(f^{\mathrm{M}} - \hat{f}^{\mathrm{M}}\right)^2 + \left(f^{\mathrm{R}}\right)^2 + \left(\hat{f}^{\mathrm{R}}\right)^2 - 2\frac{\boldsymbol{\rho}_{\mathrm{s}}\left(f^{\mathrm{I}}, \boldsymbol{x}^{\mathrm{I}}\right)}{\sqrt{\boldsymbol{N}^{\mathrm{T}}\boldsymbol{r}^{(\mathrm{s})}\boldsymbol{r}^{(\mathrm{s})\mathrm{T}}\boldsymbol{N}}}\mathrm{diag}\left(\sqrt{\boldsymbol{r}_i^{(\mathrm{s})}\boldsymbol{r}_i^{(\mathrm{s})\mathrm{T}}}\right)\boldsymbol{N}\cdot f^{\mathrm{R}}\hat{f}^{\mathrm{R}} \tag{75}$$

Moreover

$$\frac{\sqrt{\boldsymbol{r}_i^{(\mathrm{s})}\boldsymbol{r}_i^{(\mathrm{s})\mathrm{T}}}}{\sqrt{\boldsymbol{N}^{\mathrm{T}}\boldsymbol{r}^{(\mathrm{s})}\boldsymbol{r}^{(\mathrm{s})\mathrm{T}}\boldsymbol{N}}} = \frac{\boldsymbol{x}^{\mathrm{R}}}{\hat{f}^{\mathrm{R}}} \tag{76}$$

Finally, e can be calculated as:

$$e = \left(f^{\mathrm{M}} - \boldsymbol{M}\boldsymbol{m}\right)^2 + \left(f^{\mathrm{R}}\right)^2 + \boldsymbol{N}^{\mathrm{T}}\boldsymbol{C}_{\boldsymbol{x}^{\mathrm{I}}\boldsymbol{x}^{\mathrm{I}}}\boldsymbol{N} - 2\boldsymbol{\rho}_{\mathrm{s}}\left(f^{\mathrm{I}}, \boldsymbol{x}^{\mathrm{I}}\right)\cdot\mathrm{diag}\left(f^{\mathrm{R}}x_n{}^{\mathrm{R}}\right)\cdot\boldsymbol{N} \tag{77}$$

Appendix B: Approach to take samples in a MEM domain

The characteristic matrix $\boldsymbol{G}$ to describe a MEM can be decomposed by eigenvalue decomposition as:

$$\boldsymbol{G} = \boldsymbol{C}^{-1} = \boldsymbol{Q}^{\mathrm{T}}\boldsymbol{D}\boldsymbol{Q} \tag{78}$$

where $\boldsymbol{D}$ is eigenvalue matrix; $\boldsymbol{Q}$ is eigenvector matrix, and $\boldsymbol{Q}^{\mathrm{T}}\boldsymbol{Q} = \boldsymbol{I}$. The samples, $\boldsymbol{x}^{(\mathrm{s})}$, uniformly distributed in a 'multidimensional ellipsoid' can be obtained through a transformation (79) from the sampling points, $\boldsymbol{U}^{(\mathrm{s})}$, uniformly distributed in a unit hyper-sphere[28]

$$\boldsymbol{x}^{(\mathrm{s})} = \boldsymbol{x}^{\mathrm{M}} + \boldsymbol{Q}^{\mathrm{T}}\boldsymbol{D}^{-\frac{1}{2}}\boldsymbol{U}^{(\mathrm{s})} \tag{79}$$

where $\boldsymbol{x}^{\mathrm{M}}$ are the middle points of the interval variables. For a k-dimensional problem, every single set of sampling points $\boldsymbol{U}^{(\mathrm{s})}$ can be calculated in the spherical coordinates (r, θ_1, θ_2, …, $\theta_{k\text{-}1}$) as:

$$\boldsymbol{U}^{(\mathrm{s})} = \begin{bmatrix} r^{(\mathrm{s})}\cos\theta_1^{(\mathrm{s})} \\ r^{(\mathrm{s})}\sin\theta_1^{(\mathrm{s})}\cos\theta_2^{(\mathrm{s})} \\ r^{(\mathrm{s})}\sin\theta_1^{(\mathrm{s})}\sin\theta_2^{(\mathrm{s})}\cos\theta_3^{(\mathrm{s})} \\ \vdots \\ r^{(\mathrm{s})}\sin\theta_1^{(\mathrm{s})}\sin\theta_2^{(\mathrm{s})}\cdots\sin\theta_{k-2}{}^{(\mathrm{s})}\cos\theta_{k-1}{}^{(\mathrm{s})} \\ r^{(\mathrm{s})}\sin\theta_1^{(\mathrm{s})}\sin\theta_2^{(\mathrm{s})}\cdots\sin\theta_{k-2}{}^{(\mathrm{s})}\sin\theta_{k-1}{}^{(\mathrm{s})} \end{bmatrix} \tag{80}$$

where $r^{(\mathrm{s})}$ are the sampling points lie in a one-dimensional IM with range [0, 1], and [$\theta_1^{(\mathrm{s})}$, $\theta_2^{(\mathrm{s})}$, …, $\theta_{k\text{-}1}{}^{(\mathrm{s})}$] are the sampling points lie in a (k-1)-dimensional IM with range [0, 2π] of every dimension.

Finally, the sampling points in MEM domain can be obtained by taking samples in the above IMs conventionally. Incidentally, through the approach, scanning method and MC simulation can also be achieved by taking samples orthogonally and randomly, respectively.

Appendix C: Model of LV flight dynamics

The detailed expansion of LV-flight-dynamics model is expressed as

$$\begin{aligned}
\begin{bmatrix}\dot{v}_x\\ \dot{v}_y\\ \dot{v}_z\end{bmatrix} &= \frac{1}{m}\boldsymbol{G}_{\mathrm{B}}\begin{bmatrix}P-X_{\mathrm{c}}\\ Y_{\mathrm{c}}\\ Z_{\mathrm{c}}\end{bmatrix}+\frac{1}{m}\boldsymbol{G}_{\mathrm{V}}\begin{bmatrix}-X\\ Y\\ Z\end{bmatrix}\\
&+\frac{g_r}{r}\begin{bmatrix}x+R_{ox}\\ y+R_{oy}\\ z+R_{oz}\end{bmatrix}+\frac{g_{\omega e}}{\omega_e}\begin{bmatrix}\omega_{ex}\\ \omega_{ey}\\ \omega_{ez}\end{bmatrix}-\boldsymbol{A}\begin{bmatrix}x+R_{ox}\\ y+R_{oy}\\ z+R_{oz}\end{bmatrix}-\boldsymbol{B}\begin{bmatrix}v_x\\ v_y\\ v_z\end{bmatrix}\\
\begin{bmatrix}\dot{x}\\ \dot{y}\\ \dot{z}\end{bmatrix} &= \begin{bmatrix}v_x\\ v_y\\ v_z\end{bmatrix}
\end{aligned} \tag{81}$$

where m is the mass of LV; $[P, 0, 0]^{\mathrm{T}}$ is the component of propulsion $\boldsymbol{P}$, $[X_{\mathrm{c}}, Y_{\mathrm{c}}, Z_{\mathrm{c}}]^{\mathrm{T}}$ are the components of control force $\boldsymbol{F}_{\mathrm{c}}$; $[X, Y, Z]^{\mathrm{T}}$ are the components of aerodynamic force $\boldsymbol{R}$, which can be calculated as:

$$\begin{cases} X = C_x q S_{\mathrm{R}} \\ Y = C_y^{\alpha} q S_{\mathrm{R}} \alpha \\ Z = -C_y^{\alpha} q S_{\mathrm{R}} \beta \end{cases} \tag{82}$$

where α and β are the angle of attack and sideslip angle, respectively. C_x is drag coefficient, and C_y^{α} is the derivative of the lift-coefficient with respect to α; S_{R} is the reference surface area; q is the dynamic pressure, which is calculated as:

$$q = \frac{1}{2}\rho v^2 \tag{83}$$

where ρ is the atmospheric density, and v is the resultant velocity of the LV flight as

$$v = \sqrt{v_x^2 + v_y^2 + v_z^2} \tag{84}$$

Then, $\boldsymbol{G}_{\mathrm{B}}$ and $\boldsymbol{G}_{\mathrm{V}}$ are coordinate-transform matrixes as:

$$\begin{aligned}
\boldsymbol{G}_B &= \begin{bmatrix}\cos\varphi\cos\psi & -\sin\varphi & \cos\varphi\sin\psi\\ \sin\varphi\cos\psi & \cos\varphi & \sin\varphi\sin\psi\\ -\sin\psi & 0 & \cos\psi\end{bmatrix}\\
\boldsymbol{G}_{\mathrm{V}} &= \begin{bmatrix}\cos\theta\cos\sigma & -\sin\theta & \cos\theta\sin\sigma\\ \sin\theta\cos\sigma & \cos\theta & \sin\theta\sin\sigma\\ -\sin\sigma & 0 & \cos\sigma\end{bmatrix}
\end{aligned} \tag{85}$$

where φ and ψ are, respectively, the pitch angel and yaw angel, which describe the flight attitude of the LV. Meanwhile, θ and σ are, respectively, flight path angle and flight path azimuth angle, which describe the flight direction of the LV. These angles can be derived as:

$$\begin{cases} \theta = \arctan\dfrac{v_y}{v_x} \\ \sigma = -\arcsin\dfrac{v_z}{v} \\ \varphi = \theta + \alpha \\ \psi = \sigma + \beta \end{cases} \tag{86}$$

Moreover, $\boldsymbol{A}$ and $\boldsymbol{B}$, in(81), are the matrixes to describe inertial force caused by the earth rotation as

$$\boldsymbol{A}=\begin{bmatrix} \omega_{ex}{}^2-\omega_e{}^2 & \omega_{ex}\omega_{ey} & \omega_{ex}\omega_{ez} \\ \omega_{ex}\omega_{ey} & \omega_{ey}{}^2-\omega_e{}^2 & \omega_{ey}\omega_{ez} \\ \omega_{ex}\omega_{ez} & \omega_{ey}\omega_{ez} & \omega_{ez}{}^2-\omega_e{}^2 \end{bmatrix}$$
$$\boldsymbol{B}=\begin{bmatrix} 0 & -2\omega_{ez} & 2\omega_{ey} \\ 2\omega_{ez} & 0 & -2\omega_{ex} \\ -2\omega_{ey} & 2\omega_{ex} & 0 \end{bmatrix} \tag{87}$$

where ω_e is the earth-rotation rate, and $[\omega_{ex}, \omega_{ey}, \omega_{ez}]^T$ are the components of the vector $\boldsymbol{\omega}_e$. Afterwards, $[R_{0x}, R_{0y}, R_{0z}]^T$, in (81), are the components of the vector $\boldsymbol{R}_0$ to describe the position of the launch point. Next, g_r and $g_{\omega e}$ are the components of gravitational acceleration, and can be calculated as:

$$\begin{cases} g_r=-\dfrac{\mu}{r^2}\left[1+J\left(\dfrac{a_e}{r}\right)^2\left(1-5\sin^2\phi\right)\right] \\ g_{\omega e}=-2\dfrac{\mu}{r^2}J\left(\dfrac{a_e}{r}\right)^2\sin\phi \end{cases} \tag{88}$$

where μ and J are the constant characteristics of the gravity. a_e the length of the semi-major axis of earth under an ellipsoid model, besides, the semi-minor axis is symbolled by b_e. And, r, the geocentric distance of the LV, is calculated as:

$$r=\sqrt{(x+R_{ox})^2+(y+R_{oy})^2+(z+R_{oz})^2} \tag{89}$$

Meanwhile, ϕ, the geocentric latitudinal, can be derived from:

$$\sin\phi=\frac{(x+R_{ox})\omega_{ex}+(y+R_{oy})\omega_{ey}+(z+R_{oz})\omega_{ez}}{r\omega_e} \tag{90}$$

In addition, the flight height of the LV can also be obtained by r and ϕ as:

$$h=r-\frac{a_e b_e}{\sqrt{a_e^2\sin^2\phi+b_e^2\cos^2\phi}} \tag{91}$$

Finally, these equations can be solved according to a given flight-program angle, and generally, they are provided in the form as:

$$\begin{cases} \varphi^*=\varphi_{PR}(t) \\ \psi^*=0 \end{cases} \tag{92}$$

Accordingly, to achieve the flight program, the corresponding α and β are expressed as

$$\begin{cases} \alpha=A_\varphi[(\varphi_{PR}-\omega_{ez}t-\theta)] \\ \beta=A_\psi[(\varphi_{ex}\sin\varphi-\omega_{ey}\cos\varphi)t-\sigma] \end{cases} \tag{93}$$

where A_φ and A_ψ are both constant coefficients.

Reference

1. Brake, M.R.: The role of epistemic uncertainty of contact models in the design and optimization

of mechanical systems with aleatoric uncertainty. Nonlinear Dynam. 77(3), 899-922 (2014). https://doi.org/10.1007/s11071-014-1350-0
2. Arailopoulos, A., Giagopoulos, D.: Nonlinear constitutive force model selection, update and uncertainty quantification for periodically sequential impact applications. Nonlinear Dynam. 99(4), 2623-2646 (2020). https://doi.org/10.1007/s11071-019-05444-1
3. Benedetti, K.C.B., Gonçalves, P.B.: Nonlinear response of an imperfect microcantilever static and dynamically actuated considering uncertainties and noise. Nonlinear Dynam. 107(2), 1725-1754 (2022). https://doi.org/10.1007/s11071-021-06600-2
4. ASTILL, C.J., IMOSSEIR, S.B., SHINOZUKA, M.: Impact Loading on Structures with Random Properties. Journal of Structural Mechanics 1(1), 63-77 (1972). https://doi.org/10.1080/03601217208905333
5. Geller, D.K.: Linear Covariance Techniques for Orbital Rendezvous Analysis and Autonomous Onboard Mission Planning. J. Guid. Control Dynam. 29(6), 1404-1414 (2006). https://doi.org/10.2514/1.19447
6. Jin, K., Geller, D., Luo, J.: Development and Validation of Linear Covariance Analysis Tool for Atmospheric Entry. J. Spacecraft Rockets 56(3), 854-864 (2018). https://doi.org/10.2514/1.A34297
7. REARDON, D., LEITHEAD, W.E.: Statistical linearization: a comparative study. Int. J. Control 52(5), 1083-1105 (1990). https://doi.org/10.1080/00207179008953585
8. Prabhakar, A., Fisher, J., Bhattacharya, R.: Polynomial Chaos-Based Analysis of Probabilistic Uncertainty in Hypersonic Flight Dynamics. J. Guid. Control Dynam. 33(1), 222-234 (2010). https://doi.org/10.2514/1.41551
9. Jones, B.A., Doostan, A., Born, G.H.: Nonlinear Propagation of Orbit Uncertainty Using Non-Intrusive Polynomial Chaos. J. Guid. Control Dynam. 36(2), 430-444 (2013). https://doi.org/10.2514/1.57599
10. Bhusal, R., Subbarao, K.: Generalized Polynomial Chaos Expansion Approach for Uncertainty Quantification in Small Satellite Orbital Debris Problems. The Journal of the Astronautical Sciences 67(1), 225-253 (2020). https://doi.org/10.1007/s40295-019-00176-1
11. Elishakoff, I.E., Elisseeff, P., Glegg, S.A.L.: Nonprobabilistic, convex-theoretic modeling of scatter in material properties. Aiaa J. 32, 843-849 (1994)
12. Zadeh, L.A.: Fuzzy sets as a basis for a theory of possibility. Fuzzy Set. Syst. 100, 9-34 (1999). https://doi.org/10.1016/S0165-0114(99)80004-9
13. Ben-Haim, Y., Elishakoff, I.E.: Convex models of uncertainty in applied mechanics, 1990. (1990)
14. Marano, G.C., Quaranta, G.: Robust optimum criteria for tuned mass dampers in fuzzy environments. Appl. Soft Comput. 9(4), 1232-1243 (2009). https://doi.org/10.1016/j.asoc.2009.03.010
15. Wei, S., Zhao, J., Han, Q., Chu, F.: Dynamic response analysis on torsional vibrations of wind turbine geared transmission system with uncertainty. Renew. Energ. 78, 60-67 (2015). https://doi.org/10.1016/j.renene.2014.12.062
16. Wang, Z., Tian, Q., Hu, H.: Dynamics of spatial rigid – flexible multibody systems with uncertain interval parameters. Nonlinear Dynam. 84(2), 527-548 (2016). https://doi.org/10.1007/s11071-015-2504-4

17. Peng, H., Shi, B., Wang, X., Li, C.: Interval estimation and optimization for motion trajectory of overhead crane under uncertainty. Nonlinear Dynam. 96(2), 1693-1715 (2019). https://doi.org/10.1007/s11071-019-04879-w
18. Wu, J., Zhang, Y., Chen, L., Luo, Z.: A Chebyshev interval method for nonlinear dynamic systems under uncertainty. Appl. Math. Model. 37(6), 4578-4591 (2013). https://doi.org/10.1016/j.apm.2012.09.073
19. Wu, J., Luo, Z., Zhang, Y., Zhang, N., Chen, L.: Interval uncertain method for multibody mechanical systems using Chebyshev inclusion functions. Int. J. Numer. Meth. Eng. 95(7), 608-630 (2013). https://doi.org/10.1002/nme.4525
20. Li, C., Chen, B., Peng, H., Zhang, S.: Sparse regression Chebyshev polynomial interval method for nonlinear dynamic systems under uncertainty. Appl. Math. Model. 51, 505-525 (2017). https://doi.org/10.1016/j.apm.2017.06.008
21. Fu, C., Ren, X., Yang, Y., Lu, K., Qin, W.: Steady-state response analysis of cracked rotors with uncertain-but-bounded parameters using a polynomial surrogate method. Commun. Nonlinear Sci. 68, 240-256 (2019). https://doi.org/10.1016/j.cnsns.2018.08.004
22. Fu, C., Ren, X., Yang, Y., Lu, K., Wang, Y.: Nonlinear response analysis of a rotor system with a transverse breathing crack under interval uncertainties. Int. J. Nonlin. Mech. 105, 77-87 (2018). https://doi.org/10.1016/j.ijnonlinmec.2018.07.001
23. Wang, L., Chen, Z., Yang, G.: A polynomial chaos expansion approach for nonlinear dynamic systems with interval uncertainty. Nonlinear Dynam. 101(4), 2489-2508 (2020). https://doi.org/10.1007/s11071-020-05895-x
24. Wang, L., Yang, G.: An interval uncertainty propagation method using polynomial chaos expansion and its application in complicated multibody dynamic systems. Nonlinear Dynam. 105(1), 837-858 (2021). https://doi.org/10.1007/s11071-021-06512-1
25. Jiang, C., Zhang, Q.F., Han, X., Liu, J., Hu, D.A.: Multidimensional parallelepiped model—a new type of non-probabilistic convex model for structural uncertainty analysis. Int. J. Numer. Meth. Eng. 103(1), 31-59 (2015). https://doi.org/10.1002/nme.4877
26. Ni, B.Y., Jiang, C., Han, X.: An improved multidimensional parallelepiped non-probabilistic model for structural uncertainty analysis. Appl. Math. Model. 40(7), 4727-4745 (2016). https://doi.org/10.1016/j.apm.2015.11.047
27. Jiang, C., Han, X., Lu, G.Y., Liu, J., Zhang, Z., Bai, Y.C.: Correlation analysis of non-probabilistic convex model and corresponding structural reliability technique. Comput. Method. Appl. M. 200(33), 2528-2546 (2011). https://doi.org/10.1016/j.cma.2011.04.007
28. Jiang, C., Ni, B.Y., Han, X., Tao, Y.R.: Non-probabilistic convex model process: A new method of time-variant uncertainty analysis and its application to structural dynamic reliability problems. Comput. Method. Appl. M. 268, 656-676 (2014). https://doi.org/10.1016/j.cma.2013.10.016
29. Jiang, C., Li, J.W., Ni, B.Y., Fang, T.: Some significant improvements for interval process model and non-random vibration analysis method. Comput. Method. Appl. M. 357, 112565 (2019). https://doi.org/10.1016/j.cma.2019.07.034
30. Jiang, C., Liu, N.Y., Ni, B.Y.: A Monte Carlo simulation method for non-random vibration analysis. Acta Mech. 228(7), 2631-2653 (2017). https://doi.org/10.1007/s00707-017-1842-3

31. Ni, B.Y., Jiang, C., Li, J.W., Tian, W.Y.: Interval K-L expansion of interval process model for dynamic uncertainty analysis. J. Sound Vib. 474, 115254 (2020). https://doi.org/10.1016/j.jsv.2020.115254
32. Fragkoulis, V.C., Kougioumtzoglou, I.A., Pantelous, A.A.: Statistical Linearization of Nonlinear Structural Systems with Singular Matrices. J. Eng. Mech. 142(9), 4016063 (2016). https://doi.org/10.1061/(ASCE)EM.1943-7889.0001119
33. Ni, B.Y., Jiang, C., Huang, Z.L.: Discussions on non-probabilistic convex modelling for uncertain problems. Appl. Math. Model. 59, 54-85 (2018). https://doi.org/10.1016/j.apm.2018.01.026
34. Jiang, C., Ni, B.Y., Liu, N.Y., Han, X., Liu, J.: Interval process model and non-random vibration analysis. J. Sound Vib. 373, 104-131 (2016). https://doi.org/10.1016/j.jsv.2016.03.019
35. Wu, J., Luo, Z., Zhang, N., Zhang, Y.: A new sampling scheme for developing metamodels with the zeros of Chebyshev polynomials. Eng. Optimiz. 47(9), 1264-1288 (2015). https://doi.org/10.1080/0305215X.2014.963071
36. Li, J., Jiang, C., Ni, B., Zhan, L.: Uncertain vibration analysis based on the conceptions of differential and integral of interval process. Int. J. Mech. Mater. Des. 16(2), 225-244 (2020). https://doi.org/10.1007/s10999-019-09470-0
37. Brevault, L., Balesdent, M.: Uncertainty quantification for multidisciplinary launch vehicle design using model order reduction and spectral methods. Acta Astronaut. 187, 295-314 (2021). https://doi.org/10.1016/j.actaastro.2021.06.040
38. Zhao, J., Li, H., He, X., Huang, Y., Liu, J., Lo Schiavo, A.: Uncertainty Analysis for Return Trajectory of Vertical Takeoff and Vertical Landing Reusable Launch Vehicle. Math. Probl. Eng. 2020, 4313758 (2020). https://doi.org/10.1155/2020/4313758
39. Zheng, X., Ma, N., Gao, C., Jing, W.: Propagation mechanism analysis of navigation errors caused by initial state errors for long-range vehicles. Aerosp. Sci. Technol. 67, 378-386 (2017). https://doi.org/10.1016/j.ast.2017.04.016

Statements and declarations

Funding

The present work was supported by the major advanced research project of Civil Aerospace from State Administration of Science, Technology and Industry of China.

Competing Interests

On behalf of all authors, the corresponding author states that there is no conflict of interest.

Data Availability

The complete source code (written in MATLAB) of the method applied in the two numerical tests and the LV-ascent-trajectory problem, as well as the source code of corresponding MC analyses, are provided in the supplementary material.

The source code of the MCLM applied in Duffing oscillator analysis, Vehicle ride analysis and the Problem 1 and the Problem 2 of LV ascent trajectory in the folder “MCLM”, which are respectively named as:

“CMLM_Duffing.m”,

“CMLM_VehicleRide.m”,

“CMLM_LVtrajectory_1stStage.m”,

“CMLM_LVtrajectory_2nd3rdStage.m”.

The source code of the MCS for Duffing oscillator analysis, Vehicle ride analysis and the Problem 1 and the Problem 2 of LV ascent trajectory in the folder “MCS”, which are respectively named as:

“MCS_Duffing.m”,

“MCS_VehicleRide.m”,

“MCS_LVtrajectory_1stStage.m”,

“MCS_LVtrajectory_2nd3rdStage.m”.

Supplementary Files

This is a list of supplementary files associated with this preprint. Click to download.

- sourcecode.rar